Chapter VII: Structure and Magnetic Properties of $Ti_{1-x}Co_xO_{2-\delta}$ Thin Films After Swift Heavy Ion Irradiation

In the previous chapters, we have discussed the structural and magnetic properties of $Ti_{1-x}Co_xO_2$ nanoparticles as well as thin films under the influence of defects like oxygen vacancies. Creation of defects during synthesis or deposition can be controlled by the growth parameters. However, it is difficult to introduce defects after the synthesis or deposition. The present chapter describes the creation of post-deposition defects made by Swift Heavy Ions (SHI) and its effect on structural, magnetic and transport behaviour of $Ti_{1-x}Co_xO_{2-\delta}$ thin films. Section 7.1 describes the condition of swift heavy ion irradiation. Structural and magnetic properties of 100 MeV Ag^{7+} ion irradiated $Ti_{1-x}Co_xO_{2-\delta}$ thin films deposited on Si substrate are discussed in Section 7.2. In addition to structural and magnetic properties, the evolution of transport and magneto-transport properties of epitaxial $Ti_{1-x}Co_xO_{2-\delta}$ thin films grown on $LaAlO_3$ substrates under the different ion fluence have been discussed in Section 7.3. Section 7.4 summarizes the experimental findings.

7.1 Conditions of Swift Heavy Ion Irradiation

To create post-deposition defects, swift heavy ion irradiation (SHI) is a unique tool as one can control the defect concentration by properly choosing the ion, energy and fluence. A brief idea about the ion matter interaction is given in Chapter I. The variation of electronic energy loss (S_e) and nuclear energy loss (S_n) with incident projectile energy (for Ag ion) is shown as Fig. 7.1 using SRIM code [Ziegler, J. F. and Biersack (2008)]. In case of S_e greater than a certain material dependent threshold value (S_{eth}), columnar defects (latent tracks) are formed. Fig.7.1 shows 100 MeV silver ions correspond to S_e ~ 18.16 keV/nm, S_n ~ 90.86 eV/ nm, and projected range (R_p) ~ 965 nm. As S_e is much higher than the S_{eth} (6.2 keV/nm for TiO_2), one may expect columnar defects (latent tracks). As R_p is much higher than the film thickness, the projectile ions will get implanted deep inside the substrate. In this Chapter, we have studied the modification in structure and magnetic properties of the thin films deposited by technique as discussed in Chapter V by creating post

deposition defects through irradiating them with 100 MeV Ag^{7+} swift heavy ions (SHI) with different fluence ($5x10^{10}$ to $1x10^{13}$ ions/cm^2). Since, Co concentration is relatively less we assume the selected ions can effectively tunnel through the thin films as well. Here we discuss the structural and magnetic properties of $Ti_{1-x}Co_xO_{2-\delta}$ (x= 0, 0.05) thin films grown on Si substrate by PLD technique. For the characterisation we have used GAXRD, SPM and SQUID magnetometry.

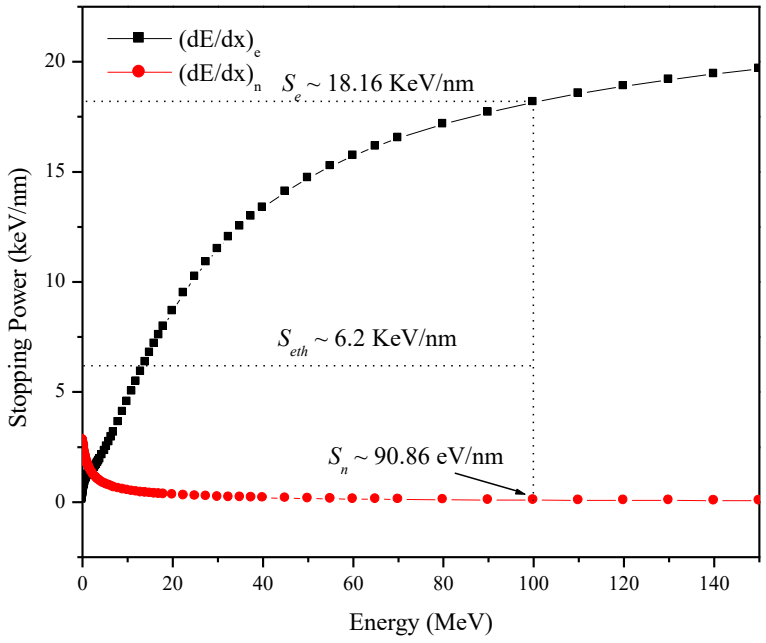

Fig.7.1 Electronic and Nuclear energy loss as a function of energy for silver ion on TiO_2 target.

7.2 Structural and Magnetic Properties Irradiated $Ti_{1-x}Co_xO_{2-\delta}$ Thin Films Deposited on Si Substrate

7.2.1Structural Properties

Glancing angle x-ray diffraction (GAXRD) pattern of $TiO_{2-\delta}$ thin films deposited under vacuum (0 mTorr), 0.1 mTorr, 1 mTorr and 300 mTorr oxygen partial pressure with different ion fluence is shown as Fig.7.2. The phase of the

pristine films changes with oxygen partial pressure. The film deposited in vacuum (without oxygen) is highly non-stoichiometric and the crystallographic phase does not resemble with either anatase or rutile phases of the TiO_2 and assigned to be non-stoichiometric Ti_4O_7 phase. Upon ion irradiation, we observe successive decrease in the XRD peak intensity of the thin films with increase in ion fluence from $5x10^{10}$ to $1x10^{13}$ ions/cm^2. We have observed neither anatase to rutile phase transformation nor recrystallization from the amorphous thin films with ion irradiation [Rath et al. (2009); Thakurdesai et al. (2009)].

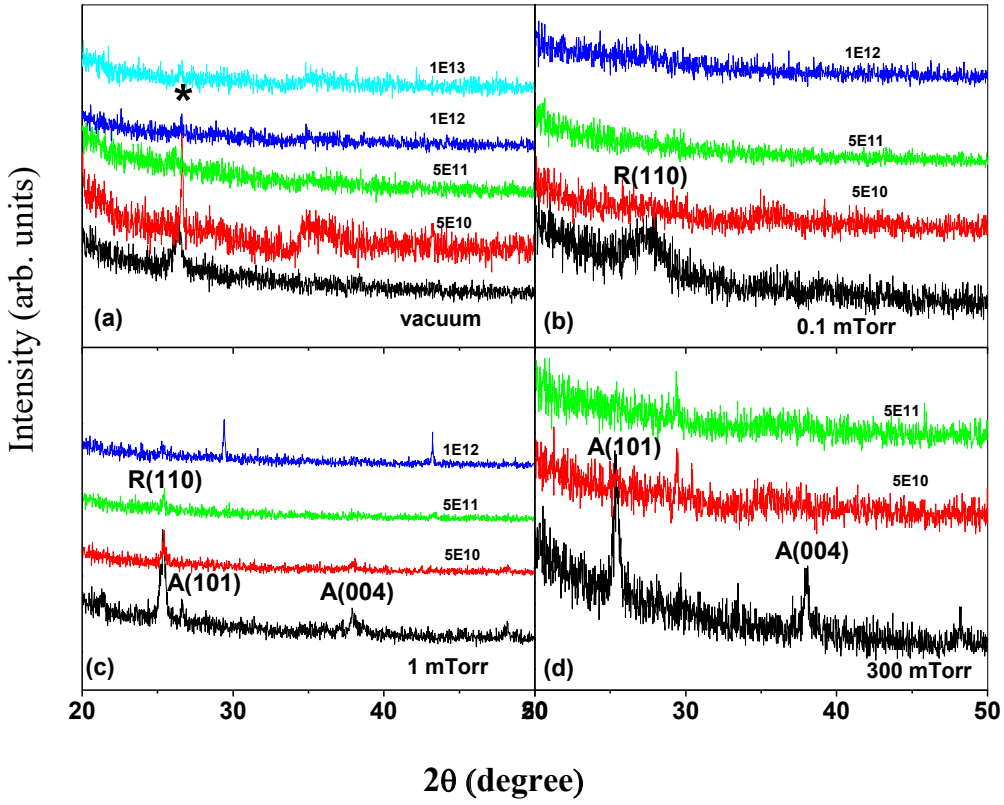

Fig.7.2 Glancing angle x-ray diffraction (GAXRD) of the TiO_2 film deposited at (a) vacuum, (b) 0.1 mTorr (c) 1 mTorr and (d) 300 mTorr oxygen partial pressure followed by ion irradiation with different fluence.

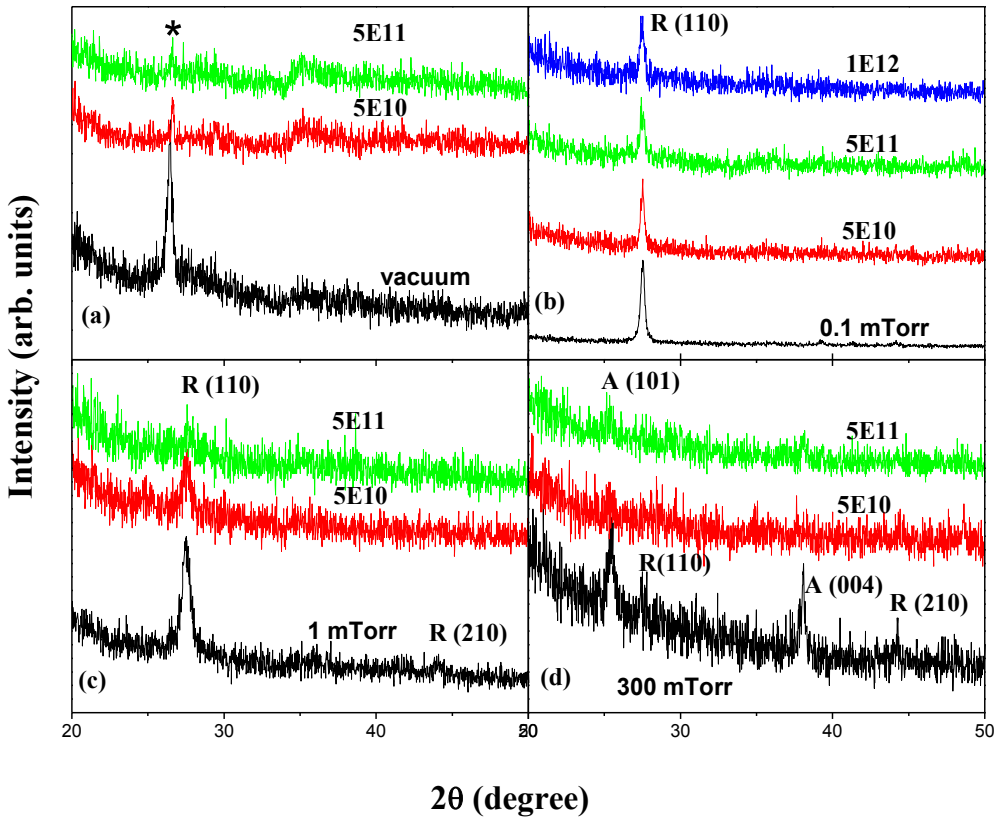

Fig. 7.3 Glancing angle x-ray diffraction (GAXRD) of the film deposited at (a) vacuum, (b) 0.1 mTorr (c) 1 mTorr and (d) 300 mTorr oxygen partial pressure followed by ion irradiation with different fluence.

The GAXRD pattern of $Ti_{1-x}Co_xO_{2-\delta}$ (x=0.015) films deposited under various oxygen partial pressures (pristine) irradiated with different fluence is shown as Fig.7.2. Rutile phase forms at low oxygen partial pressure whereas a mixed phase of anatase and rutile is formed at 300 mTorr. The cause of such anomaly in phase formation in TiO_2 and Co-doped TiO_2 (CTO) thin films with deposition pressure is attributed to difference in oxygen vacancies during deposition as discussed in detail in Chapter V [Mohanty et al. (2012)]. Among all the films, GAXRD clearly reveals that the film deposited under 0.1 mTorr oxygen partial pressure retains its crystallinity upto a fluence of 1 x 10^{12} ions/cm^2 (Fig.7. 2 (b)) whereas all other films get amorphized at the same fluence. As the S_e of 100 MeV Ag^{7+} ions substantially exceed the threshold electronic energy loss value, S_{eth} for amorphized latent track formation in TiO_2,

amorphization of the films occur with ion fluence [Nomura et al. (2003)]. This amorphization can be explained on the basis of Coulomb explosion or thermal spike model of ion track formation [Fleisher et al. (1975)].

In Coulomb explosion model, a dense positive charged zone of target material, produced around the ion path by electronic excitation on a time scale of 10^{-15}-10^{-14} s, explodes as a consequence of Coulomb repulsion before electrical neutrality is achieved. The thermal spike model describes the transport of energy out of a heated region surrounding the ion path. The thermal spike involves local thermalization in the electronic system in about 10^{-14}s. Energy locked to the electrons is then transferred to the lattice by electron-phonon coupling in the time scale of 10^{-14} - 10^{-12}s leading to a large increase in lattice temperature. Mostly it leads to the formation of amorphized latent tracks due to melting and quenching of the lattice [Toulemonde et al. (2000)]. There are reports where it has been shown that anatase phase of TiO_2 transforms to rutile phase after SHI irradiation [Rath et al. (2009)]. Such transformation occurs if the thermal spike temperature T_s exceeds the phase transition temperature T_p, where T_s in oxide system has been estimated to be ~ 1000 °C [Avasthi et al. (2000)]. Sometimes, SHI is effective to crystallize the material from amorphous phase [Thakurdesai et al. (2008)]. However, in the present case we do not observe any such phase transformation rather successive degradation of crystallinity of the films. The films deposited at 0.1 and 1 mTorr oxygen partial pressure have rutile structure which is thermodynamically stable, so T_s cannot modify their phase. The film deposited at 0.1 mTorr oxygen partial pressure possesses higher crystallinty as well as demonstrates resistance to ion irradiation upto the fluence 1 x 10^{12} ions/cm^2. On comparison of the GAXRD patterns of the pristine films, the CTO film deposited under 0.1 mTorr oxygen partial pressure demonstrates higher degree of crystalinity with radiation resistant behaviour. Hence, we restrict our studies on the irradiated films deposited at 0.1 mTorr oxygen partial pressure.

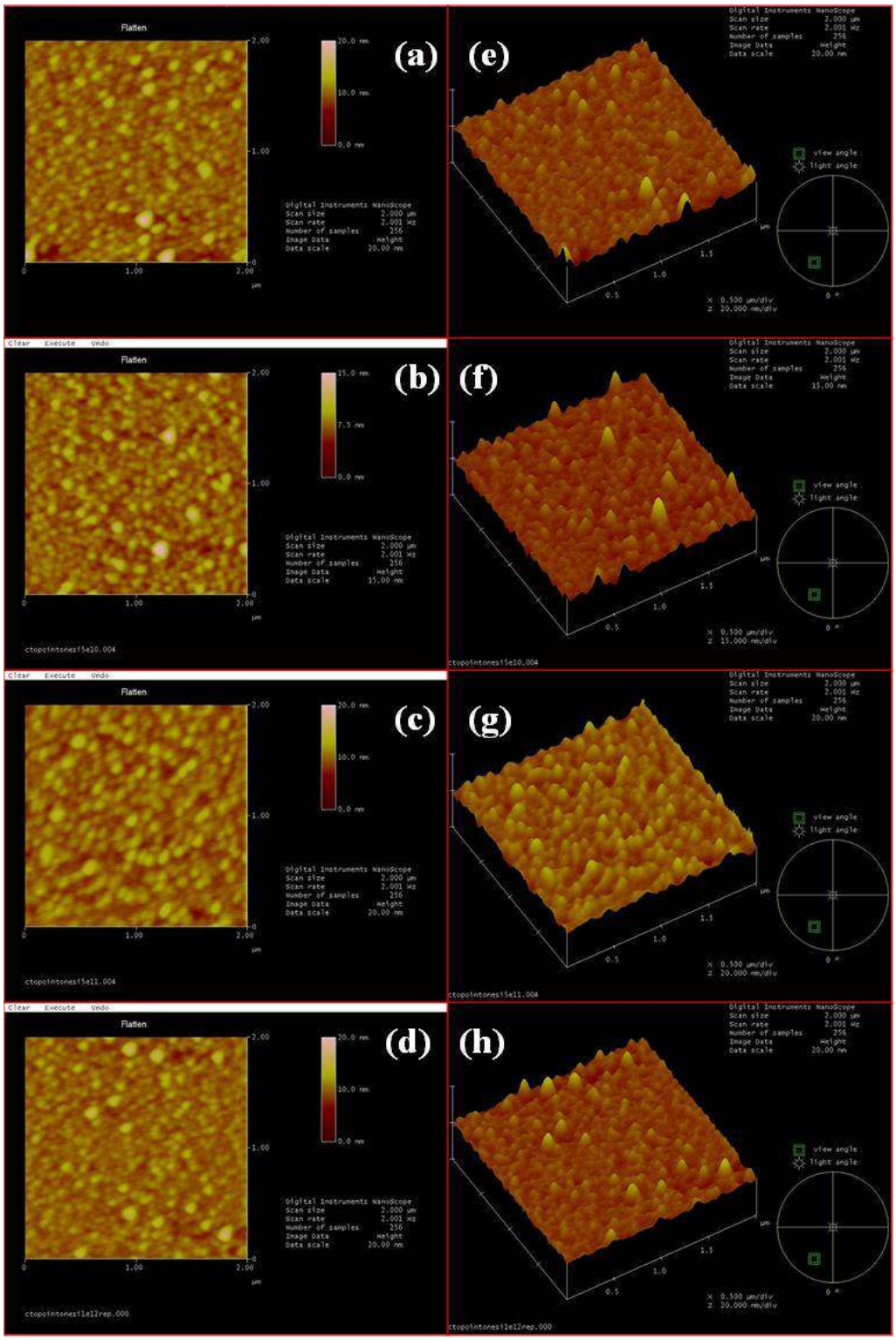

Fig.7.4 SPM image of the film CTO film deposited at 0.1 mTorr oxygen partial pressure with irradiation fluence (a) pristine, (b) 5 x 10^{10} ions/cm^2, (c) 5x 10^{11} ions/cm^2, (d) 5x 10^{12} ions/cm^2. Figures (e) to (h) depict the 3D representation of the respective films.

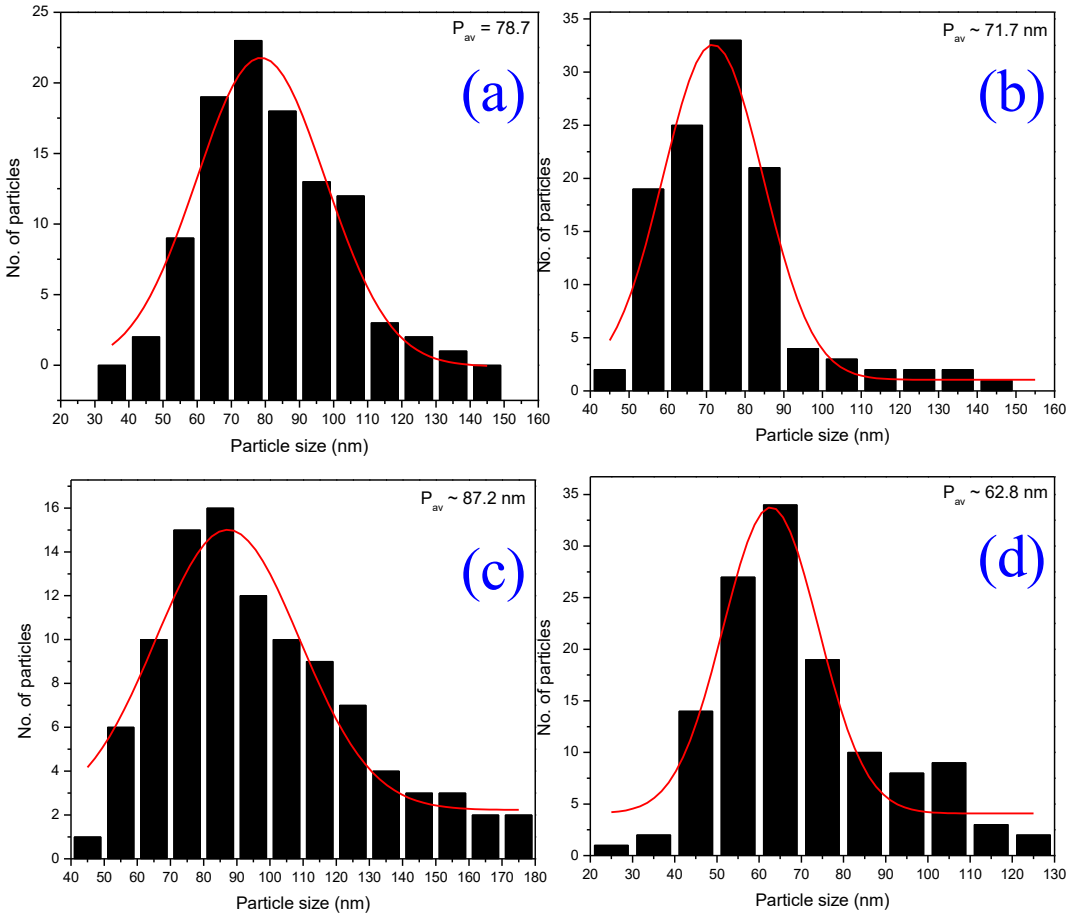

Fig.7.5 Particle size histogram of Co-doped TiO_2 film deposited under 0.1 mTorr oxygen partial pressure and irradiated with 100 MeV Ag^{7+} ion with fluence (a) pristine, (b) $5x10^{10}$ ions/cm^2, (c) $5x10^{11}$ ions/cm^2, and (d) $1x10^{12}$ ions/cm^2.

The surface morphology of the pristine as well as irradiated CTO films deposited at 0.1 mTorr oxygen partial pressure is studied with scanning probe microscopy. Fig.7.4 (a) to (d) depicts the 2D surface topography of the pristine and irradiated films with various fluence. Fig.7. 4 (e) to (h) gives the 3D representation of the aforementioned films. The scan surfaces are equal to 2μm x 2μm in size. From the SPM of the films, it is clear that the films are composed of particles of nano-size. With ion irradiation, we observe a change in surface topography. Fig.7.5 illustrates the particle size distribution histogram

for the pristine as well as irradiated films. The average particle size measured from the histogram varies from 62 nm to 87 nm. However, the crystallite size calculated from the x-ray line width using Scherrer formula for the pristine as well as irradiated films varies from 24 nm to 29 nm. Comparing the crystallite size with average particle size, it is confirmed that particles are of polycrystalline in nature. The surface roughness calculated from the SPM is found to decrease from 14.4 nm to 11.2 nm after irradiating 100 MeV Ag^{7+} ions with fluence 1 x 10^{12} ions/cm^2.

The fluence dependence of x-ray peak intensity shows exponential decay behaviour. By assuming that the tracks occupy part of the specimen volume, the peak intensity for any crystallographic reflection can be expressed by Poisson's law as mentioned below:

$$I(\varphi) = I_0 \exp(-A\varphi) \qquad (7.1)$$

Where I (φ) denote the intensity of the XRD peak as a function of ion-fluence φ, I_0 is the intensity before irradiation (pristine film) and A is the damage cross section of a single ion track [Ishikawa et al. (2006)]. By fitting the decrease in x-ray peak intensity ((110) reflection of rutile) as a function of fluence following Eq. (1), the average diameter (D) of the tracks is found to be ~ 4.2 nm (Fig. 7. 6). Similar track diameter calculation from the decreasing x-ray intensity has been reported by Ishikawa et al. (2006).

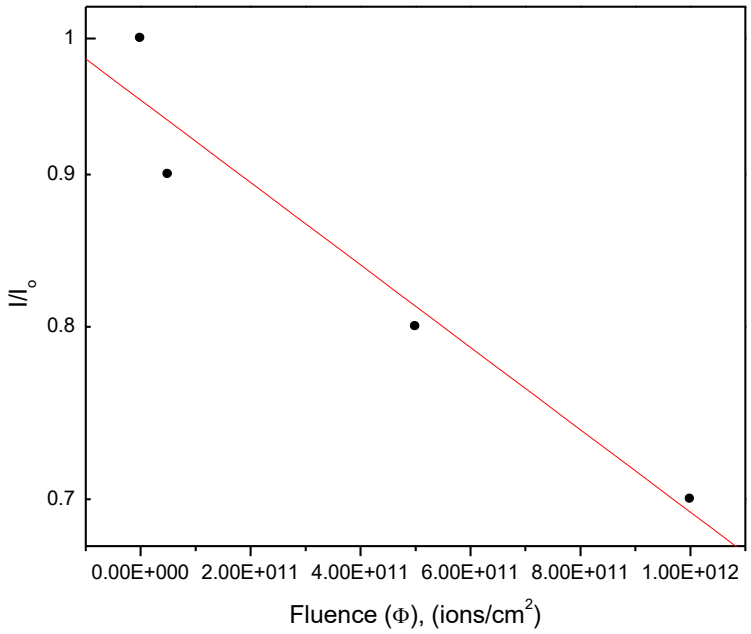

Fig.7.6 Logarithm of the intensity of (110) peak of anatase TiO_2, $\ln(I/I_0)$, plotted against fluence, φ, where $I = I(\varphi)$ is the peak intensity for the irradiated sample and I_0 is the peak intensity before irradiation. Straight line is to demonstrate that peak intensity decreases following Poisson's law according to Eq. (7.1).

7.2.2 Magnetic Properties

The pristine $TiO_{2-\delta}$ films become amorphous after ion irradiation and their magnetic measurements do not yield feasible values. In case of CTO films, the film deposited at 0.1 mTorr oxygen partial pressure has the highest magnetic moment, and it is the only film that survives upon ion irradiation. Hence the pristine and irradiated CTO films deposited at 0.1mTorr are used for the magnetic measurements. Magnetisation (*M*) as a function of applied magnetic field (*H*) is measured at room temperature using SQUID Magnetometer (MPMS-XL, Quantum Design, USA) in reciprocating sample option (RSO) mode. The *M* vs. *H* plots of the pristine and irradiated films 7 demonstrate increase in magnetisation with applied magnetic field that saturates at higher field (Fig.7.7). With reversing the field, magnetisation does

not follow the same path showing a hysteresis loop. The presence of loop at room temperature thus confirms the ferromagnetic behaviour in films irradiated at all fluences. It is further evident that although coercivity remains almost same, the saturation magnetisation (M_s) decreases with increase in ion fluence (Fig.7.7). Thakur et al. (2011) have reported the ferromagnetism in paramagnetic TiO_2 thin film followed by a phase transformation from anatase to rutile and brookite mixed phase by silver ion irradiation of energy 200 MeV. The ferromagnetism is explained on the basis of distortion in TiO_6 octahedra due to ion irradiation [Thakur et al. (2011)]. Zhou et al. (2009) demonstrated room temperature ferromagnetism in TiO_2 single crystals irradiated with 2 MeV oxygen ions. Recently, Sanyal et al. (2014) reported 4 MeV Ar^{5+} irradiated polycrystalline TiO_2 films show ferromagnetic ordering due to defects.

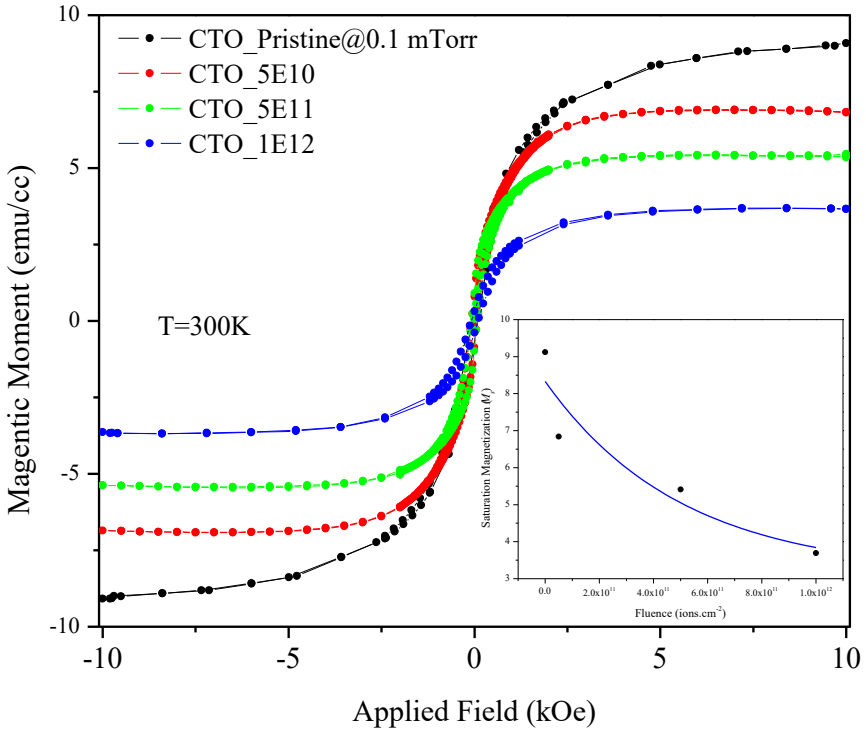

Fig.7.7 Magnetisation (M) as a function of applied magnetic field (H) for the pristine and irradiated Co-doped TiO_2 film deposited at 0.1 mTorr oxygen partial pressure. The inset (a) shows the exponential decrease in the saturation magnetisation with increase in ion fluence.

Saturation magnetisation (M_s) versus fluence shown in inset (a) of Fig.7.7 indicates an exponential decay of M_s with ion fluence. We believe, with ion irradiation similar to amorphized latent tracks, disordered magnetic regions are also formed, which have negligible contribution to saturation magnetisation (M_s). We explain the reduction in M_s as a consequence of decrease in the fraction of the material surrounding the ion path contributing to magnetism. Like the fitting of x-ray intensity as a function of fluence, we have also fitted the M_s with ion fluence using Poisson's equation as given below.

$$M(\varphi) = M_0 \exp(-A_1\varphi) \qquad (7.2)$$

Where M (φ) is the saturation magnetisation of the film as a function of ion fluence φ. M_0 is the initial magnetisation and A_1 is the cross-section of the magnetic disordered region. The fitting of the data to the above equation yields linear behaviour (Fig.7. 8). The diameter is found to be ~ 6.6 nm which is larger than the latent track diameter ~ 4.2 nm measured from the XRD data. A pictorial representation of the ion tracks surrounded by the magnetic disordered region is depicted in Fig.7.9. We propose, with ion irradiation not only the material shows structural disorder but also demonstrates magnetic disorder which is having higher diameter than the ion tracks.

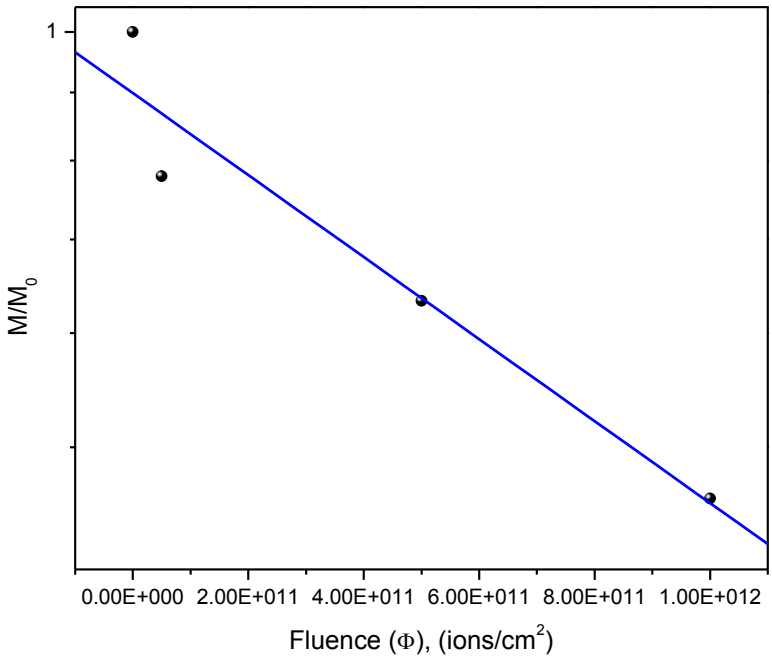

Fig.7.8 Logarithm of the saturation magnetisation (M_s) of anatase TiO_2 film deposited at 0.1 mTorr oxygen partial pressure, $\ln(M/M_0)$, plotted against fluence, φ, where M = M(φ) is the saturation magnetisation of the irradiated sample and M_0 is the saturation magnetisation of the pristine film. Straight line fitting in inset (b) is to demonstrate that saturation magnetisation decreases following Poisson's law according to Eq. (7.2).

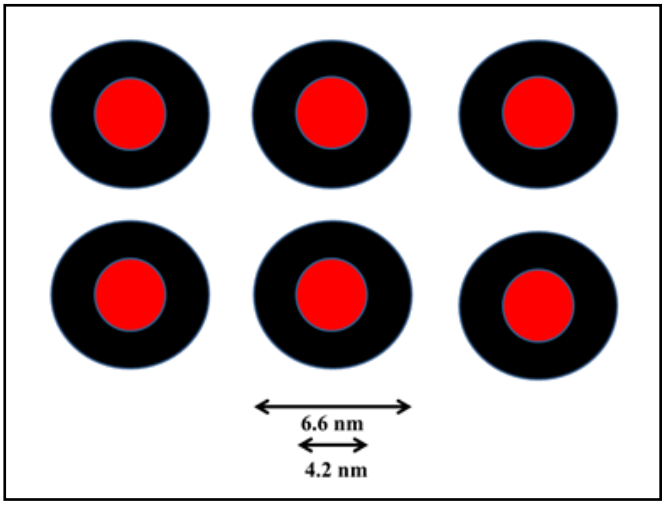

Fig.7.9 Schematic representation of the ion track regions. The red core indicates the amorphized latent track region whereas the black circle represents the extent of magnetic disordered region over the surface of the film.

7.3 Structural, Magnetic, Transport and Magneto-transport Properties of Irradiated $Ti_{1-x}Co_xO_{2-\delta}$ Thin Films Deposited on $LaAlO_3$ Substrate

In the previous section, we have discussed the structure and magnetic properties of polycrystalline $Ti_{1-x}Co_xO_{2-\delta}$ thin films. Here we discuss the effect of 100 MeV Ag^{7+} ions on structural and magnetic properties of epitaxial $Ti_{1-x}Co_xO_{2-\delta}$ (x = 0, 0.05) thin films grown on $LaAlO_3$ substrates. The properties of the pristine films are discussed in Chapter V. The resistivity of the films increases with oxygen partial pressure. Films deposited at 0.1 mTorr oxygen partial pressure are shown to have good crystalllinty as well as conducting in nature. So here we selectively studied the films deposited at 0.1 mTorr oxygen partial pressure and irradiated with $1x10^{11}$, $1x10^{12}$ and $1x10^{13}$ ions/cm^2 ion fluence. XRD, Raman, RBS, SPM and SQUID magnetometry have been used to characterise the thin films. In addition, we have studied the transport and magneto-transport properties of the pristine and irradiated thin films down to 5 K with an external magnetic field of 8Tesla. The low temperature resistivity data have been analyzed by considering thermally activated electrons model, Kondo model of scattering of electrons and the possible contribution from the Quantum Correction to Conductivity as proposed by Lee and Ramakrishna ().

7.3.1 Structural Properties

XRD pattern of the CTO thin films deposited on $LaAlO_3$ substrate with varying the oxygen partial pressure (0, 10 and 300 mTorr) is shown as Fig. 7.10. All films show anatase phase irrespective of the deposition pressure. Growth of anatase single phase on $LaAlO_3$ substrate is due to its close resemblance of the lattice parameter of the substrate (0.378 nm) and the anatase phase of TiO_2 (0.3785 nm) [Kennedy and Stampe (2003)]. XRD pattern clearly shows reflections from planes (004) and (008) and all other reflections are suppressed. Fig. 7.10 (a) and (b) depict the XRD pattern of $Ti_{0.95}Co_{0.05}O_{2-\delta}$ and $TiO_{2-\delta}$ thin films deposited at 0.1 mTorr oxygen partial pressure showing the

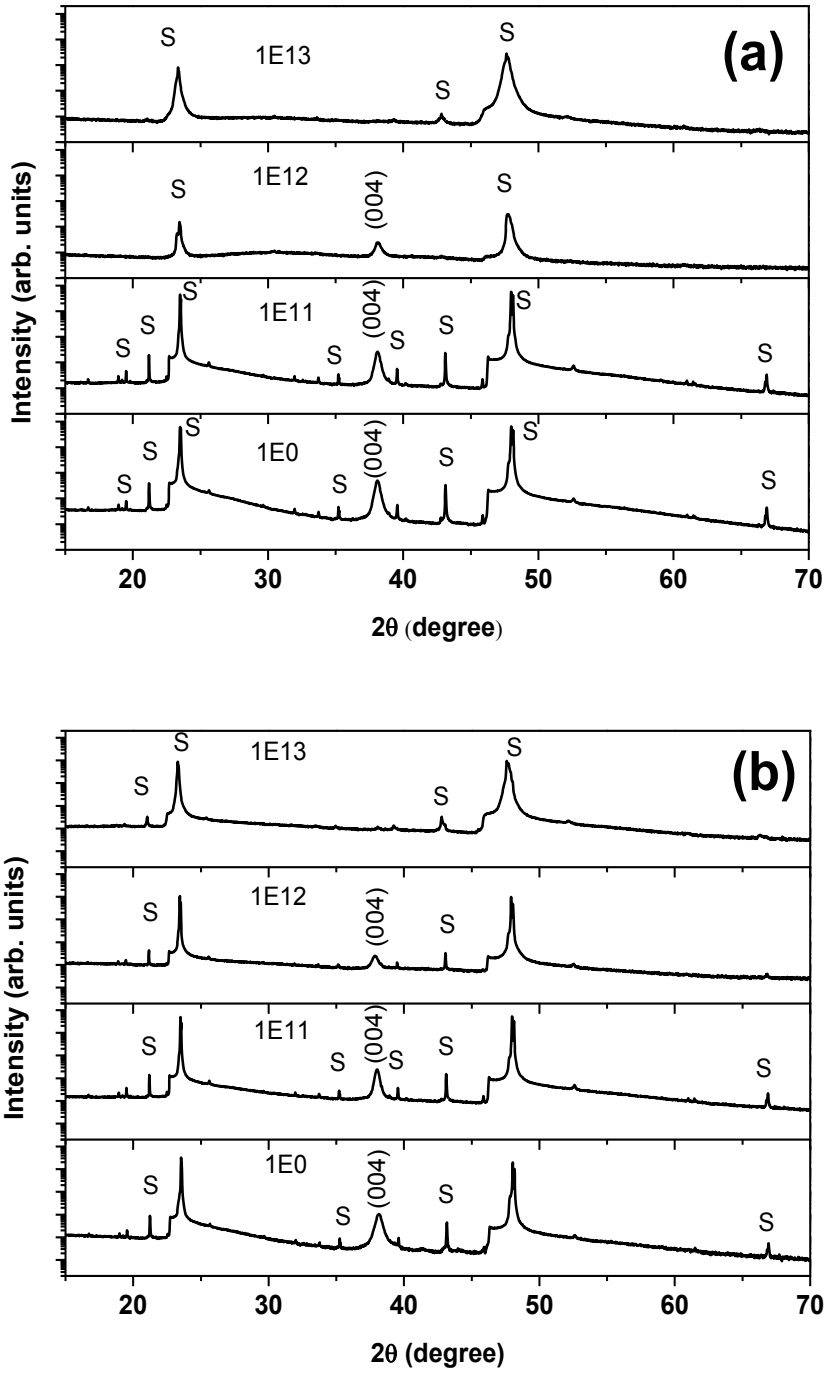

Fig.7.10 (a) X-ray diffraction pattern of $Ti_{0.95}Co_{0.05}O_{2-\delta}$ films deposited on LAO substrate under 0.1mTorr oxygen partial pressure and irradiated with 100 MeV Ag^{7+} ion with various fluence. (b) x-ray diffraction pattern of $TiO_{2-\delta}$ films deposited on $LaAlO_3$ substrate under 0.1mTorr oxygen partial pressure and irradiated with 100 MeV Ag^{7+}ion with various fluence.

effect of SHI irradiation. The films get amorphized at a fluence of $1x10^{13}$ ions/cm^2. Raman spectra of the irradiated films are depicted in Fig. 7.11 (a) and (b). Due to epitaxial nature of the as grown films, the Raman modes corresponding to the anatase phase of TiO_2 get substantially suppressed showing dominant modes of $LaAlO_3$ substrate. However, a characteristic B_{1g} mode related to anatase phase is observed for the pristine film that gradually degrades with ion fluence (Fig.7.11). Hence, both XRD and Raman results suggests the amorphization of the films with ion ion irradiation. The SPM images of the TiO_2 and $Ti_{0.95}Co_{0.05}O_{2-\delta}$ pristine and irradiated with highest fluence (1×10^{13} ions/cm^2) are shown in Fig. 7.12. From the micrographs, it is clearly evident that with ion irradiation, the surface morphology changes. In pristine TiO_2 thin film, the grains are found to be arranged in linear arrays as evident in Fig. 7.13 (e and g).

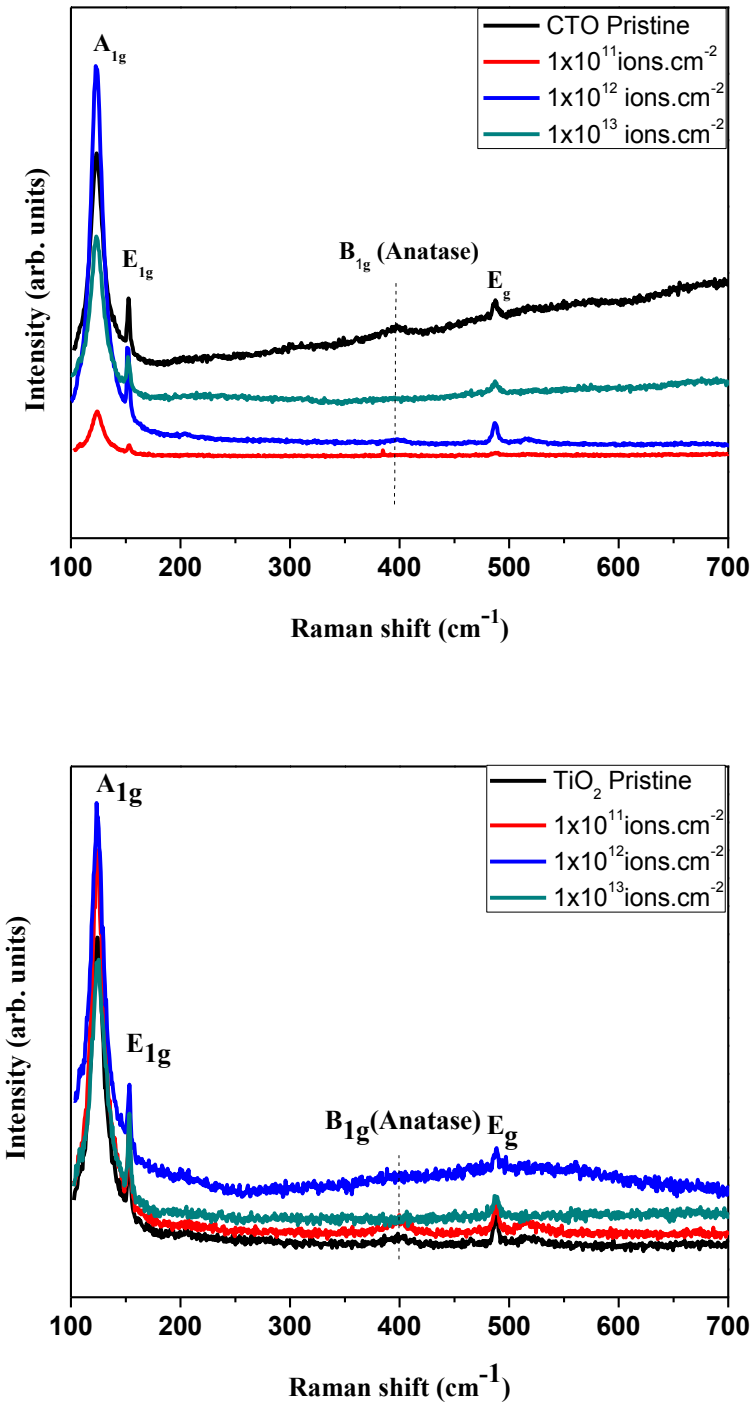

Fig.7.11(a) Raman spectra of $Ti_{0.95}Co_{0.05}O_{2-\delta}$ films deposited on LAO substrate under 0.1mTorr oxygen partial pressure and irradiated with 100 MeV Ag^{7+}ion with various fluence. (b) Raman spectra of $TiO_{2-\delta}$ films deposited on LAO substrate under 0.1mTorr oxygen partial pressure and irradiated with 100 MeV Ag^{7+}ion with various fluence.

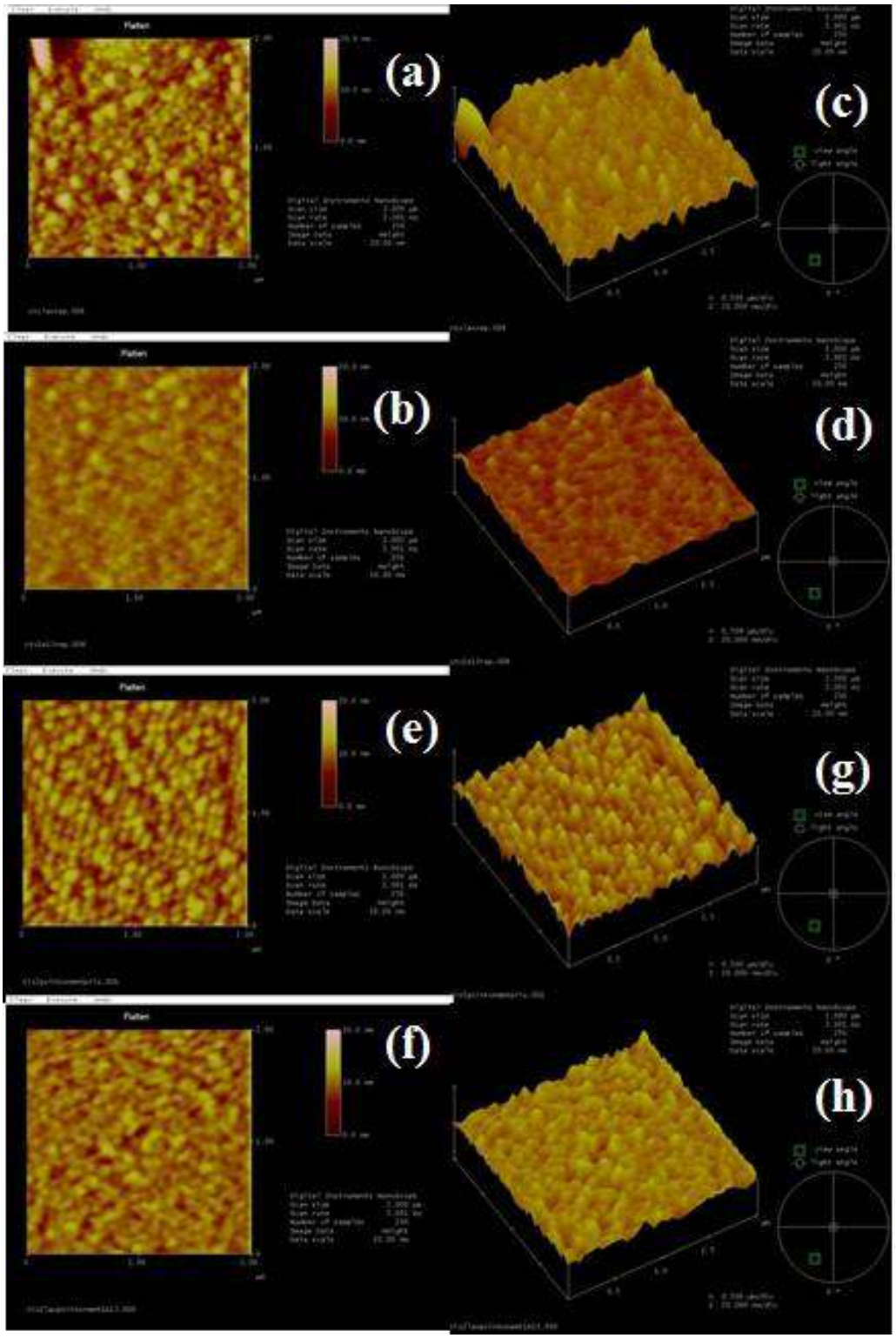

Fig.7.12 SPM images of: pristine $Ti_{0.95}Co_{0.05}O_{2-\delta}$ film (a) and film irradiated with 1 x 10^{13}ions/cm^2 (b); pristine $TiO_{2-\delta}$ film (e) and film irradiated with 1 x 10^{13}ions/cm^2. Corresponding 3D images are shown as (c), (d), (g) and (h), respectively.

7.3.2 Magnetic Properties

Magnetic behaviour of the pristine $Ti_{1-x}Co_xO_{2-\delta}$ films deposited on $LaAlO_3$ substrate by PLD technique is already discussed in Chapter V. The same sets of films are irradiated using 100 MeV Ag^{7+} ions with varying fluence. The phase of all the films are anatase and the films deposited at 0.1 mTorr demonstrate good crystallinity compared to films deposited at other oxygen partial pressure. Therefore, we have studied the role of ion irradiation on the $Ti_{1-x}Co_xO_{2-\delta}$ films deposited at 0.1mTorr oxygen partial pressure only. Magnetisation as a function of temperature is carried out using SQUID-VSM (Quantum Design, USA). The ZFC and FC magnetisation measurements with a probing field of 50 Oe for the $Ti_{1-x}Co_xO_{2-\delta}$ films are depicted in fig.7.13. The bifurcation in the ZFC and FC magnetisation curve persists upto 300 K for $Ti_{0.095}Co_{0.05}O_{2-\delta}$ pristine as well as irradiated films indicating T_c well above the room temperature (Fig.7.13 (a)). Similar irreversibility in ZFC and FC magnetisation curves for pristine and irradiated $TiO_{2-\delta}$ film is also observed (Fig.7.13 (b)). Here one may note that due to variation of the sample size, one cannot compare the magnitude of magnetic moment with irradiation for pristine and irradiated $Ti_{0.095}Co_{0.05}O_{2-\delta}$ films as shown in Fig 7.13 (a). However, careful examination of the M vs. T plots indicate the increase in difference between ZFC and FC magnetisation curves (δM), with ion fluence. This δM is maximum at 5 K for the fluence 1 $x10^{13}$ ions/cm^2. In case of $TiO_{2-\delta}$ film, δM also increases with ion fluence. A typical ZFC and FC magnetisation as a function of temperature for $TiO_{2-\delta}$ film irradiated with a fluence 1 $x10^{11}$ ions/cm^2 is shown as 7.13 (b). To further understand the effect of ion irradiation on the magnetic properties, we have carried out M vs. H measurements of the pristine and irradiated $Ti_{1-x}Co_xO_{2-\delta}$ films at 300 K as well as 5 K as shown in Fig. 7.14. Pristine as well as irradiated $Ti_{0.095}Co_{0.05}O_{2-\delta}$ films show hysteresis behaviour at both 300 and 5 K. M_s for pristine film is much higher than the pristine films deposited on Si substrate. The M_s increases for the film irradiated with 1 x 10^{11} ions/cm^2 in comparison to the pristine film at 300

K (Fig.7.14 (a)). Further, we notice a drop in M_s for the film irradiated with 1 x 10^{12} ions/cm^2 and a further increase in M_s for the film having ion fluence 1 x 10^{13} ions/cm^2. Same trend is followed for the same set of films measured at 5 K (Fig.7.14 (b)). Pristine and irradiated TiO_2 film also shows the similar M_s behaviour with ion fluence. (Fig. 7.15 (a) and (b)). In our earlier work, we have observed a systematic decrease in M_s in case of CTO films deposited on Si substrate [Chapter V]. However, in the present case, the behaviour of magnetisation with applied field is quite unique than our previous results. This shows the clear difference in magnetic behaviour in case of a film grown epitaxially than a film grown as polycrystalline one. Most important result here is that M_s for TiO_2 film irradiated at 1x10^{13} ions/cm^2 is higher than that of CTO film irradiated with same fluence. Moreover, M_s is higher in both films irradiated at highest fluence (1x10^{13} ions/cm^2) than the films having lower fluence. Although, we have shown in our previous studies that crystallinity play a vital role in deciding the ferromagnetic order , and is showing high M_s, in the present case, we do not see such effect as 1x10^{13} ions/cm^2 irradiated film is completely amorphous. To understand the unusually high magnetic moment in these irradiated films which is very different than the previously studied irradiated films grown on Si substrate, we have carried out the transport and magneto-transport measurements using four probe technique.

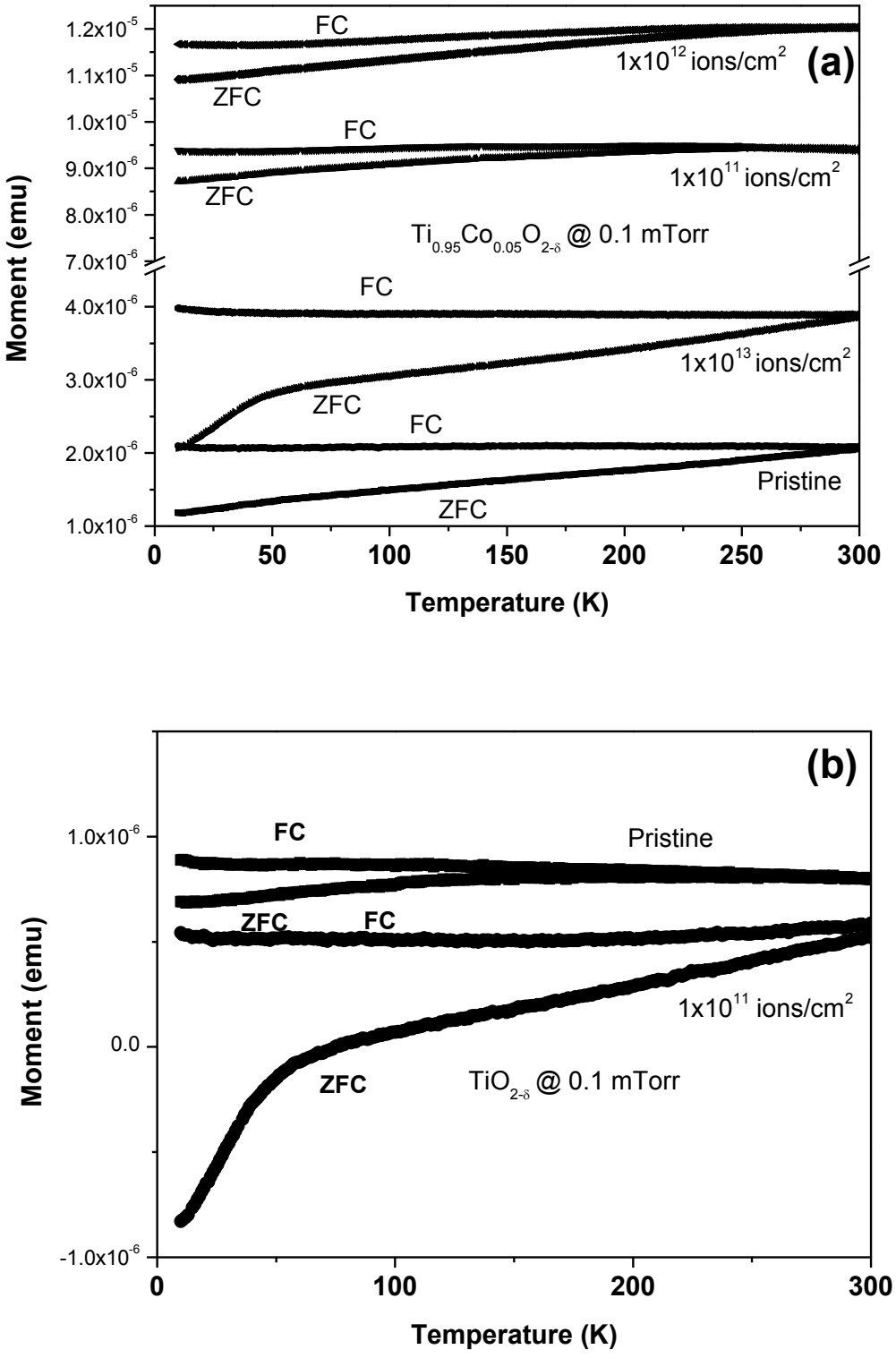

Fig.7.13 Magnetisation as a function of temperature of $Ti_{0.95}Co_{0.05}O_{2-\delta}$ (a) and $TiO_{2-\delta}$ films deposited on LAO substrate under 0.1mTorr oxygen partial pressure and irradiated with 100 MeV Ag^{7+} ions with various fluence.

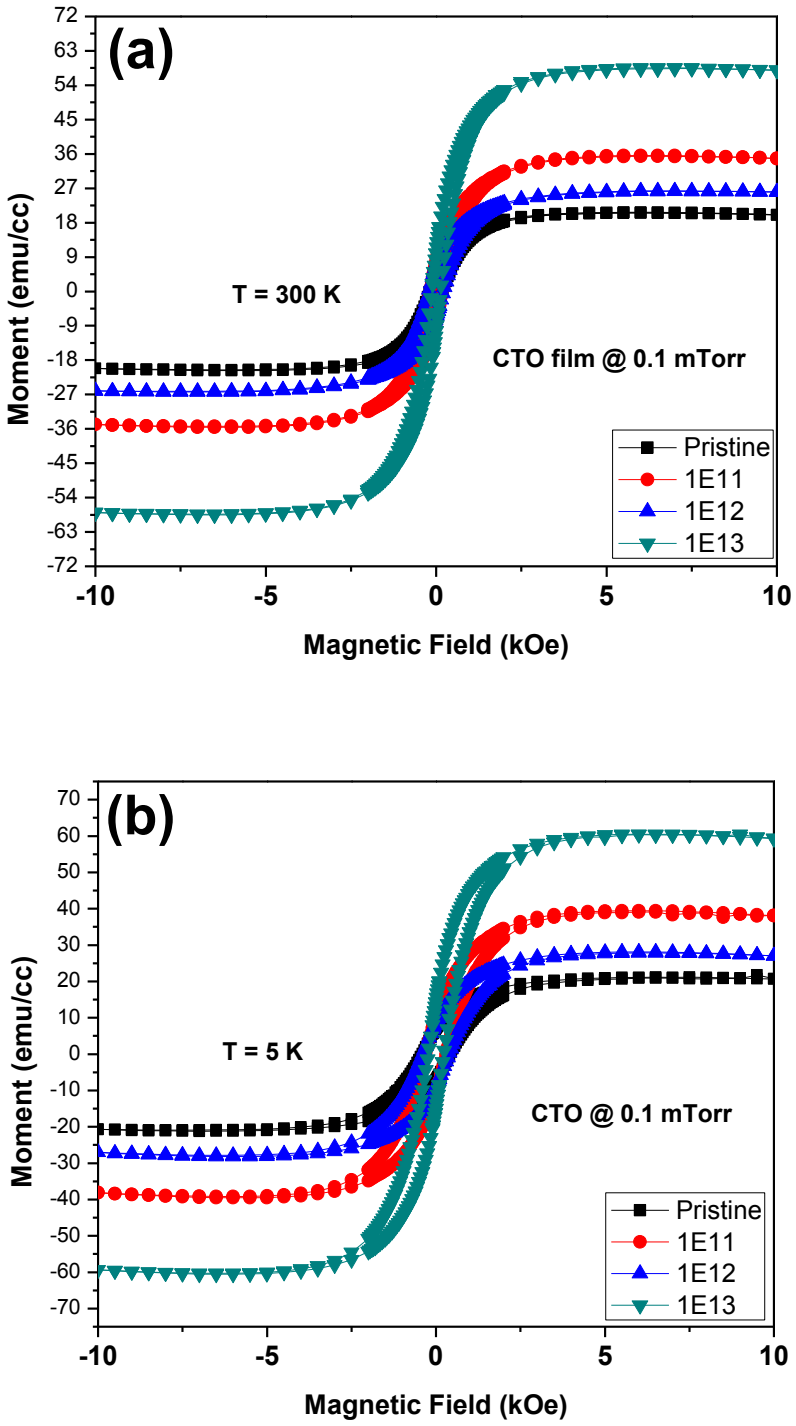

Fig.7.14(a) Magnetisation of pristine (deposited under 0.1 mTorr oxygen partial pressure) and irradiated $Ti_{0.95}Co_{0.05}O_{2-\delta}$ films as a function of applied magnetic field at 300 K. (b) Magnetisation of pristine (deposited under 0.1 mTorr oxygen partial pressure) and irradiated $Ti_{0.95}Co_{0.05}O_{2-\delta}$ films as a function of applied magnetic field at 5 K.

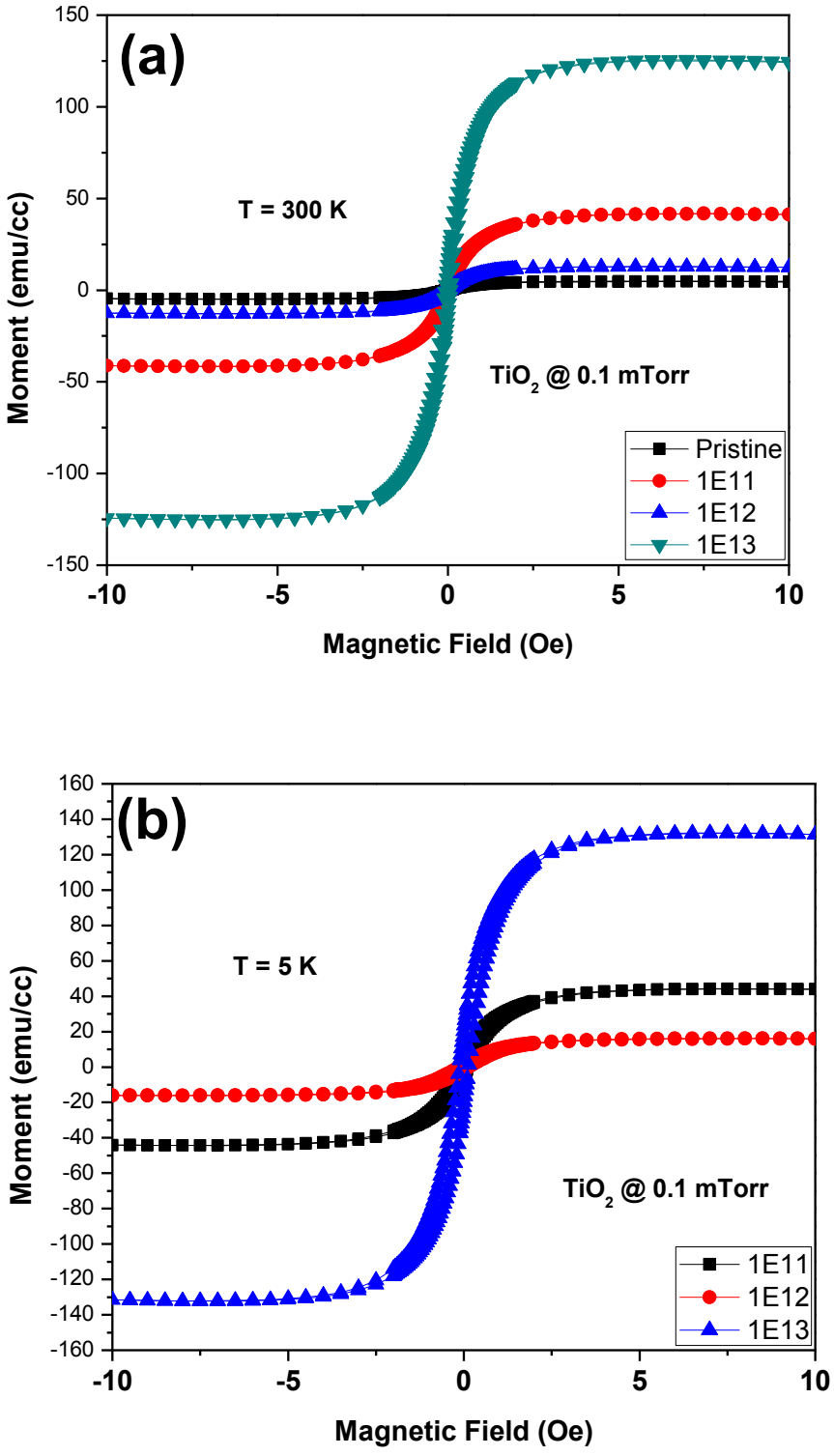

Fig.7.15(a) Magnetisation of pristine (deposited under 0.1 mTorr oxygen partial pressure) and irradiated $TiO_{2-\delta}$ films as a function of applied magnetic field at 300 K. (b) Magnetisation of pristine (deposited under 0.1 mTorr oxygen partial pressure) and irradiated $TiO_{2-\delta}$ films as a function of applied magnetic field at 5 K.

7.3.3 Transport and Magneto-transport Properties

$Ti_{0.95}Co_{0.05}O_{2-\delta}$ and $TiO_{2-\delta}$ films deposited at lowest oxygen partial pressure i.e., 0.1 mTorr are found to be conducting whereas the films deposited at 300 mTorr oxygen partial pressure are insulating with resistivity beyond the measurement limit of our system. So, we have selected to study the temperature dependent transport properties of $Ti_{0.95}Co_{0.05}O_{2-\delta}$ and $TiO_{2-\delta}$ pristine films deposited at 0.1 mTorr oxygen partial pressure as well as after irradiating with the 100 MeV Ag^{7+} ions having fluence $1x10^{11}$ and $1x10^{12}$ ions/cm^2. At fluence $1x10^{13}$ ions/cm^2, films show insulating behaviour. Fig.7.16 shows the temperature dependent resistivity of pristine $TiO_{2-\delta}$ and $Ti_{0.95}Co_{0.05}O_{2-\delta}$ films, deposited at 0.1 mTorr oxygen partial pressure. With decreasing temperature from 300 K, the resistivity gradually decreases showing a minima (T_{min}) at 115 K for $TiO_{2-\delta}$ and 103 K for $Ti_{0.95}Co_{0.05}O_{2-\delta}$ films and increases abruptly with further decreasing temperature. The minimum in resistivity is retained under application of external magnetic field of 8 Tesla (Fig.7.16). Similar to our observation, resistivity minima has also been observed by Ramaneti et al. (2007b) and Bapna et al. (2012) for Co and Fe doped TiO_2 films, respectively. Ramaneti observed the minima at 120 K for Co-doped anatase films deposited on $SrTiO_3$ (100) substrates by PLD using a $Ti_{1-x}Co_xO_2$ target with x = 0.014 [Ramaneti et al. (2007b)] and ascribed it to Kondo effect. Such effect has been attributed to a small fraction of Co isolated spins in CTO and Mn interstitials in GaMnAs with T_K around 120 K and 10 K respectively [He et al. (2005)]. This suggests a strong interaction between the Co spins and conduction electrons in the impurity band and implies that itinerant electrons and the Co local moments are in states that are energetically closer to produce such strong interaction [Ramaneti et al. (2007b)]. Minima in resistivity at low temperature have also been observed in $LaNiO_3$ and $SrRuO_3$ systems [Herranz et al (2005); Kumar et al. (2010)]. This phenomenon has been treated quantum mechanically by applying some correcting terms to the low temperature conductivity, which are popularly known as quantum corrections to conductivity (QCC) as proposed by

Lee and Ramakrishnan (1985). Earlier, a minimum in resistivity has been observed at 70 K by Chauvet et al. (1995) in anatase TiO_2 crystal grown by chemical transport reaction. They have ascribed the increase in resistivity below T_{min} due to thermally activated electrons as carriers from a donor level located at 70 K below the conduction band [Chuvet 1995]. Shinde et al. (2003) have explained the upturn in resistivity in TiO_2 and Co-doped anatase TiO_2 films, due to band like conduction in metallic regime as a consequence of possible overlap of the oxygen vacancy induced shallow donor defect level with the conduction band. It has been suggested that the transport behaviour observed in their case is due to thermal activation [Shinde et al. (2003)]. In addition to resistivity minima in both $TiO_{2-\delta}$ and $Ti_{0.95}Co_{0.05}O_{2-\delta}$ film after irradiating with fluence $1x10^{11}$ ions/cm^2, while the minima is retained in $TiO_{2-\delta}$ film, it disappears in $Ti_{0.95}Co_{0.05}O_{2-\delta}$ film (Fig.7.16). However, one can notice two clear slopes for $Ti_{0.95}Co_{0.05}O_{2-\delta}$ film (Fig 7.16). It shows a sharp increase in resistivity below 45 K. In $TiO_{2-\delta}$ film, the resistivity minima is found to decrease from 115 K to 72 K. Surprisingly, above 282 K, a decrease in resistivity with increasing temperature has been observed which is not found in $Ti_{0.95}Co_{0.05}O_{2-\delta}$ pristine films. Zhao et al. (2012) have observed similar decrease in ρ at 280 K . At higher fluence i.e. $1x10^{12}$ ions/cm^2, the minima in resistivity is found to disappear in both films demonstrating insulating behaviour (Fig.7.16). The resistivity observed for the $Ti_{0.95}Co_{0.05}O_{2-\delta}$ film at 5 K is 0.021 Ω.cm. With ion irradiation at a fluence $1x10^{11}$ ions/cm^2, it increases to 0.038 Ω.cm and abruptly increases upto 14.48 Ω.cm (i.e., 3 orders of magnitude higher). Similarly, in case of $TiO_{2-\delta}$ film the resistivity at 5 K is 0.11 Ω.cm that increases to 0.54 and 25.9 Ω.cm for the aforementioned ion fluences. Similar high resistivity phase has been observed in Bi, induced by Heavy Ions of 18O to 238U in GeV range with energy $S_e >> S_{eth}$. They explained the formation of insulating phase considering the thermal spike model [Dufour et al. (1993)]. Now if we look at the magnetic measurements, the highest magnetisation has been shown by $TiO_{2-\delta}$ film at a fluence $1x10^{13}$ions/cm^2 at 300 K as well as at 5

K. So TiO_2 having higher resistivity shows higher magnetisation. It supports our earlier assumption that, delocalisation of electrons enhances the conductivity or in another sense, in an insulating phase the defects like oxygen vacancies will rather prefer to convert Ti^{4+} to Ti^{3+}/Ti^{2+}, and hence increasing magnetism.

ρ vs. T below resistivity minima are ascribed to thermal activation, Kondo effect or explained by popular QCC model. In order to check the above criterion, we have plotted the ln (ρ) as a function of 1/T data which are shown in Fig.7.17. The ln (ρ) does not show a linear behaviour at low temperature (below T_{min}). Therefore, we eliminate the increase in resistivity below T_{min} due to thermal activation process in $TiO_{2-\delta}$ and $Ti_{0.95}Co_{0.05}O_{2-\delta}$ films (pristine and irradiated).

In our case, the films demonstrate metallic behaviour, though the resistivity is quite less than the pure metals [Kittel (1976)], there is a possibility of presence Kondo effect as reported in DMS systems like Co and Fe doped TiO_2 [Ramaneti et al. (2007b); Bapna et al. (2012)]. Kondo effect is basically observed in metallic systems having dilute magnetic impurities. We have observed the existence of minima in pristine $TiO_{2-\delta}$ and $Ti_{0.95}Co_{0.05}O_{2-\delta}$ films as well as $TiO_{2-\delta}$ film irradiated with fluence$1x10^{11}$ ions/cm^2. To check the possibility of Kondo effect in our films, we have fitted the ρ vs T data below T_{min}, using standard Kondo equation given as:

$$\rho = c\rho_0 + aT^5 - c\rho_1 \log T \quad \ldots\ldots\ldots\ldots\ldots\ldots\ldots\ldots (1)$$

where, ρ_0 is the residual resistivity, T is absolute temperature and ρ_1 is the actual resistivity and a is constant [Kittel (1976)]. The fitting is shown as Fig.7.18 with the fitting parameters tabulated in Table 7.1. However, for a Kondo system, below Kondo minima (T_K), the moment must be screened by itinerant electrons that must destroy the magnetism. That means below T_K, one should not expect ferromagnetism. However, we have observed hysteresis at 5 K below T_{min} as shown in Fig. 7.14 (b) and 7.15 (b). The authors claiming Kondo effect in similar systems does not discuss magnetic behaviour below T_K

[Ramaneti et al. (2007b); Bapna et al. (2012)]. Thus in our case, we refute the possibility of Kondo behaviour in spite of appreciable fitting of the ρ vs T data with Kondo equation. Further, similar resistivity minimum has often observed in disordered electronic systems [Herranz et al. (2005), Kumar et al. (2010)]. As DMS is like a disordered system where transition metal ions are distributed in semiconductor matrix, we have explored the same in the present case.

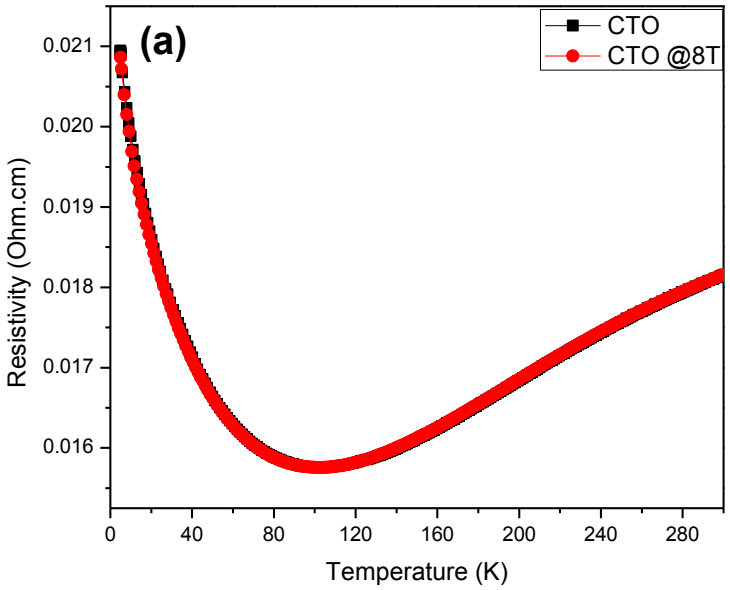

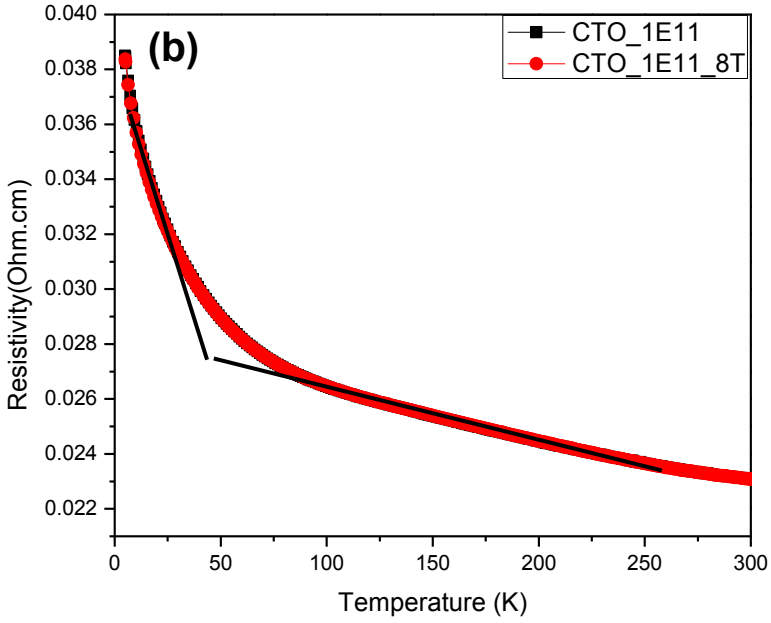

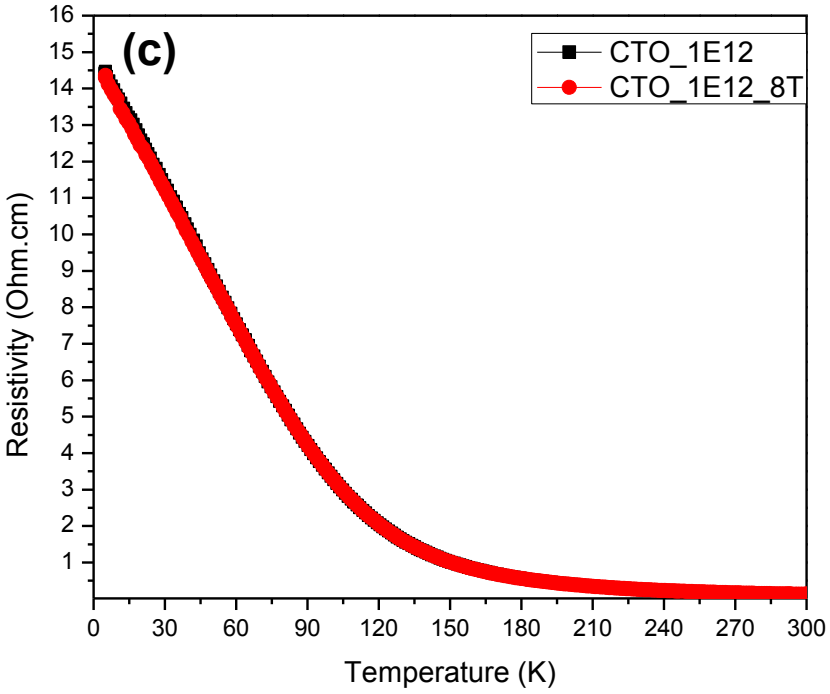
(c)
CTO_1E12
CTO_1E12_8T
Resistivity (Ohm.cm)
Temperature (K)
16
15
14
13
12
11
10
9
8
7
6
5
4
3
2
1
0
30
60
90
120
150
180
210
240
270
300

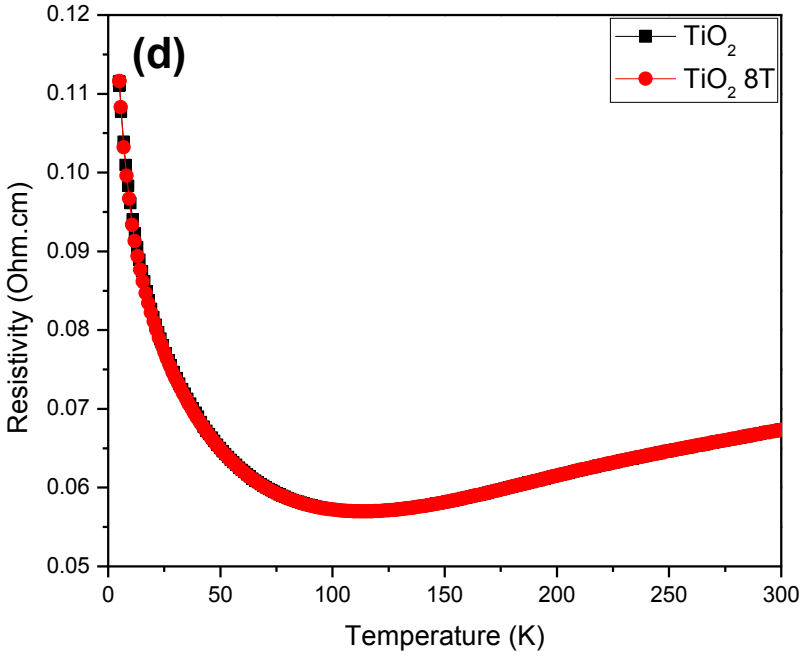
(d)
TiO2
TiO2 8T
Resistivity (Ohm.cm)
Temperature (K)
0.12
0.11
0.10
0.09
0.08
0.07
0.06
0.05
0
50
100
150
200
250
300

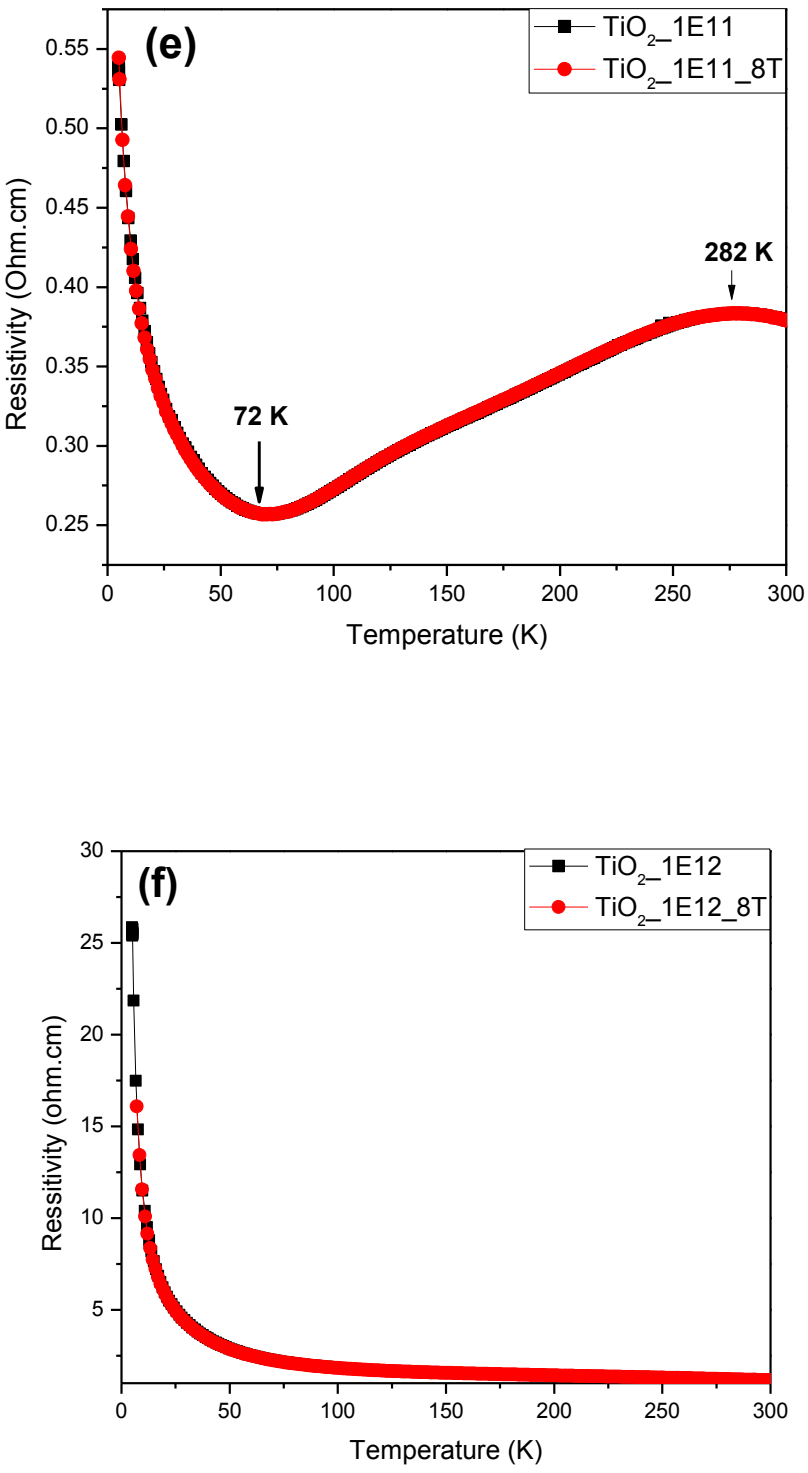

Fig.7.16 Resistivity as a function of temperature (a) CTO pristine, (b) CTO 1 x 10^{11} ions/cm^2, (c) CTO 1x10^{12} ions/cm^2 , (d) $TiO_{2-\delta}$ pristine, (e) $TiO_{2-\delta}$ 1 x 10^{11} ions/cm^2 and (f) $TiO_{2-\delta}$ 1 x 10^{12} ions/cm^2. Red symbols indicate resistivity measured as 8Tesla.

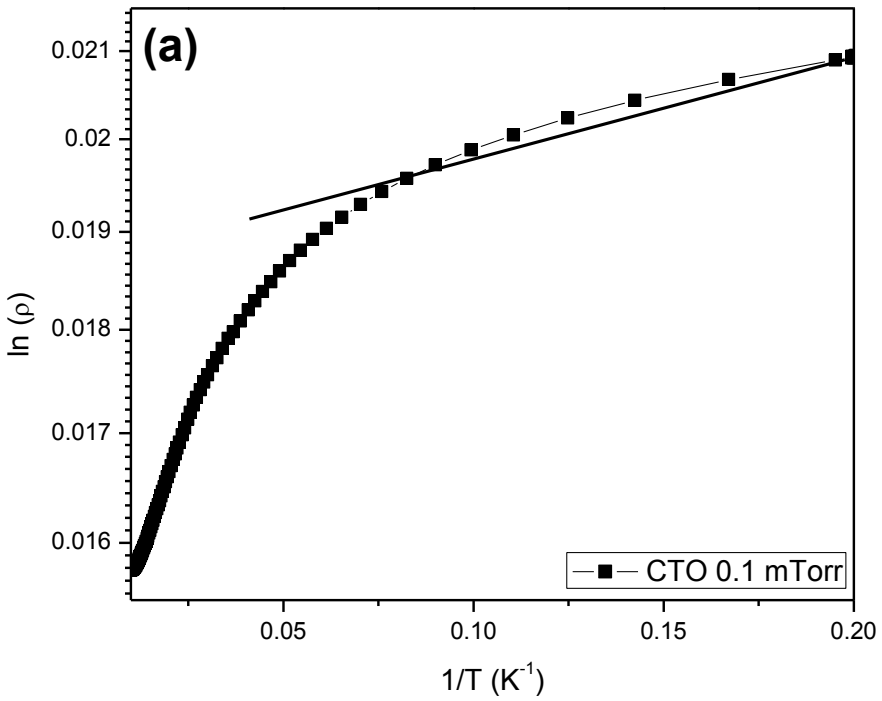
(a)
0.021
0.02
0.019
0.018
0.017
0.016
ln (ρ)
0.05
0.10
0.15
0.20
1/T (K-1)
CTO 0.1 mTorr

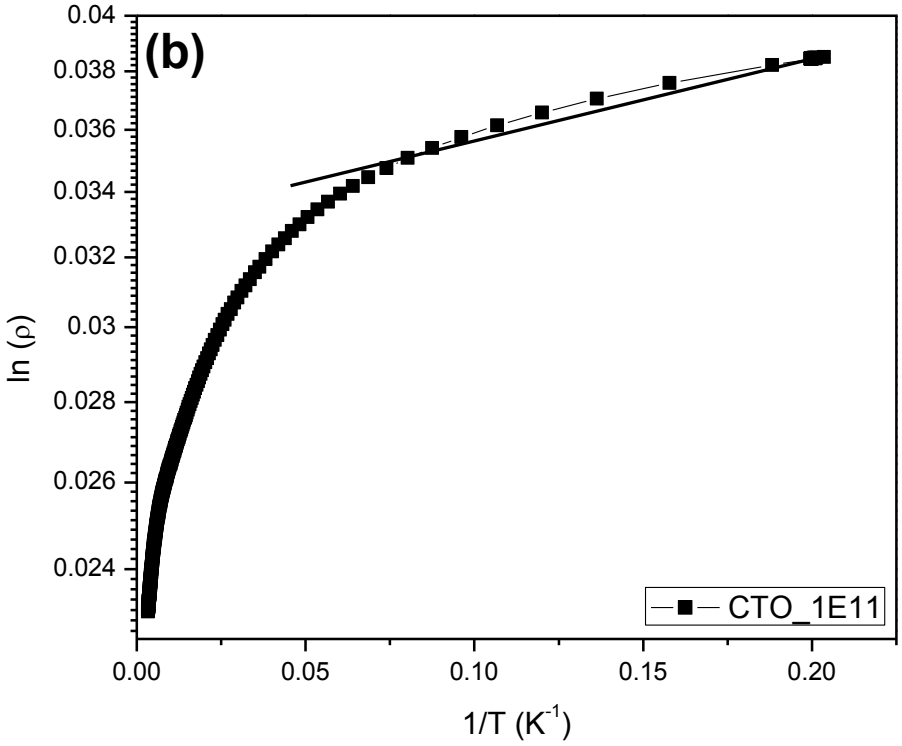
(b)
0.04
0.038
0.036
0.034
0.032
0.03
0.028
0.026
0.024
ln (ρ)
0.00
0.05
0.10
0.15
0.20
1/T (K-1)
CTO_1E11

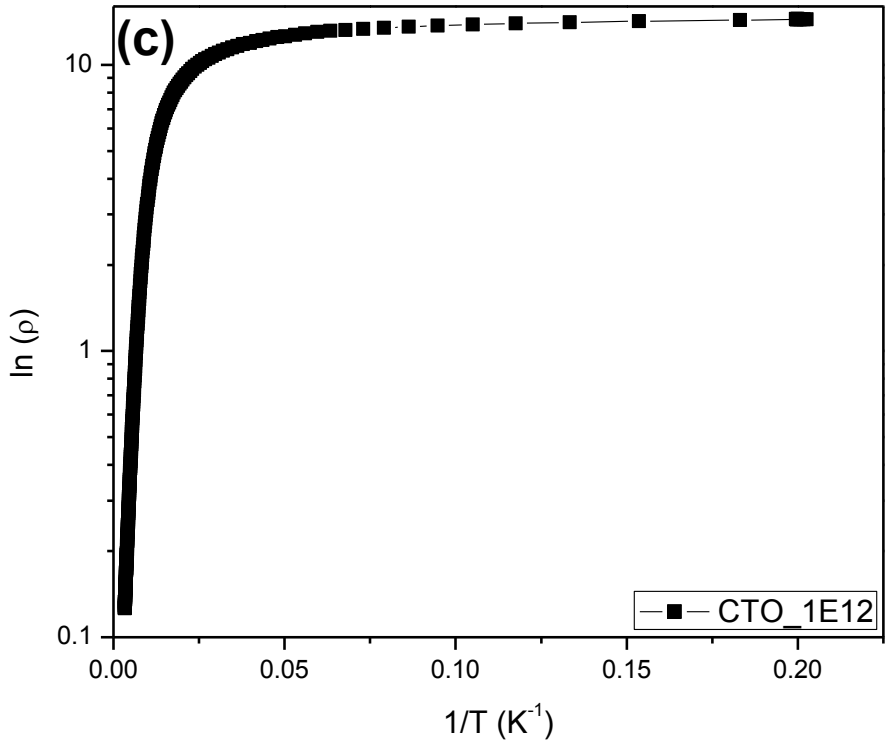
(c)
10
1
0.1
ln (ρ)
0.00
0.05
0.10
0.15
0.20
1/T (K-1)
CTO_1E12

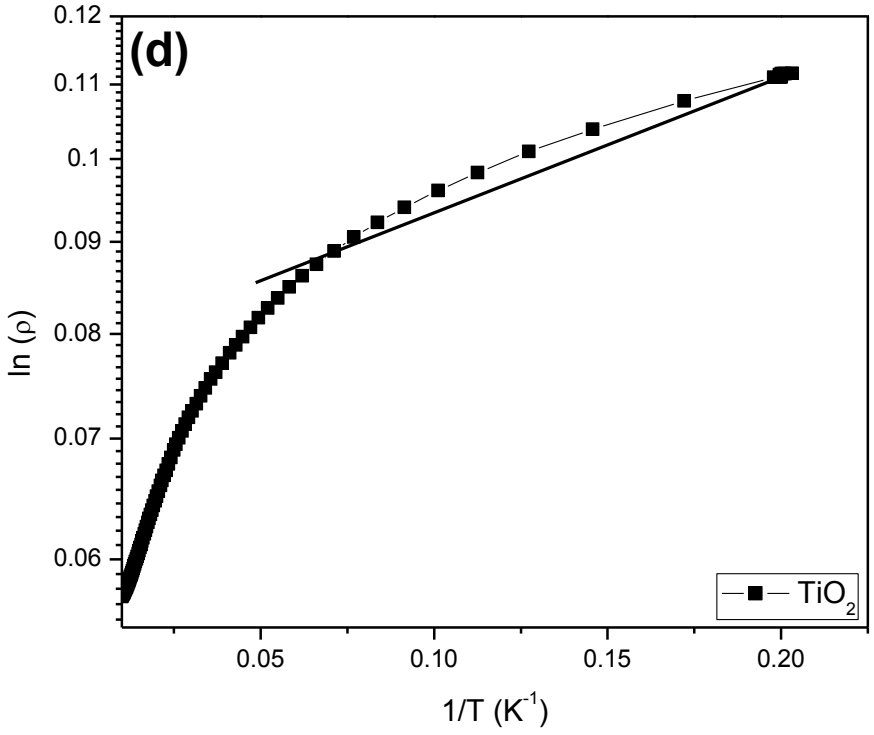
(d)
0.12
0.11
0.1
0.09
0.08
0.07
0.06
ln (ρ)
0.05
0.10
0.15
0.20
1/T (K-1)
TiO2

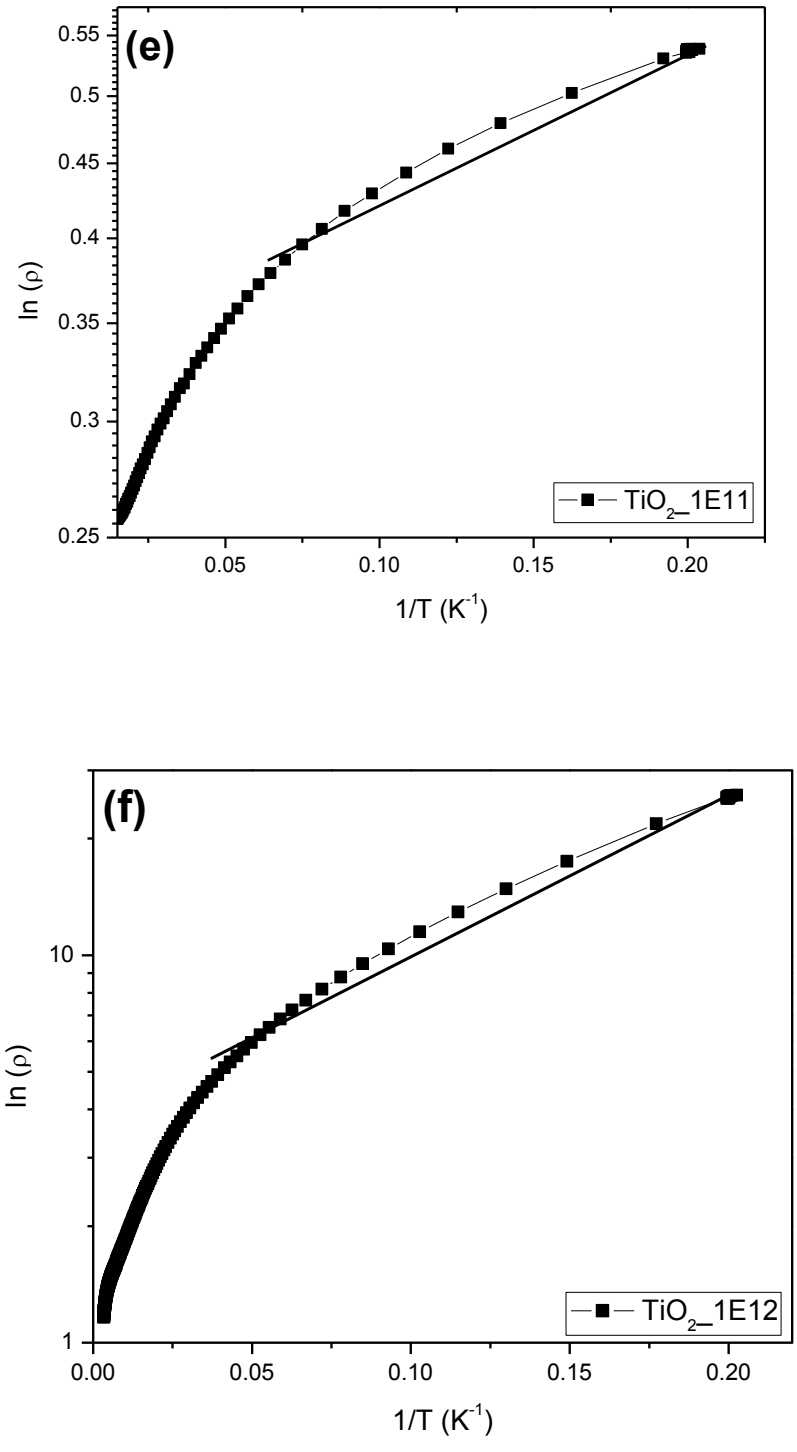

Fig.7.17 ln (ρ) as a function of 1/T (K^{-1}) for (a) CTO pristine, (b) CTO 1 x 10^{11} ions/cm^2, (c) CTO 1x10^{12} ions/cm^2 , (d) $TiO_{2-\delta}$ pristine, (e) $TiO_{2-\delta}$ 1 x 10^{11} ions/cm^2 and (f) $TiO_{2-\delta}$ 1 x 10^{12} ions/cm^2

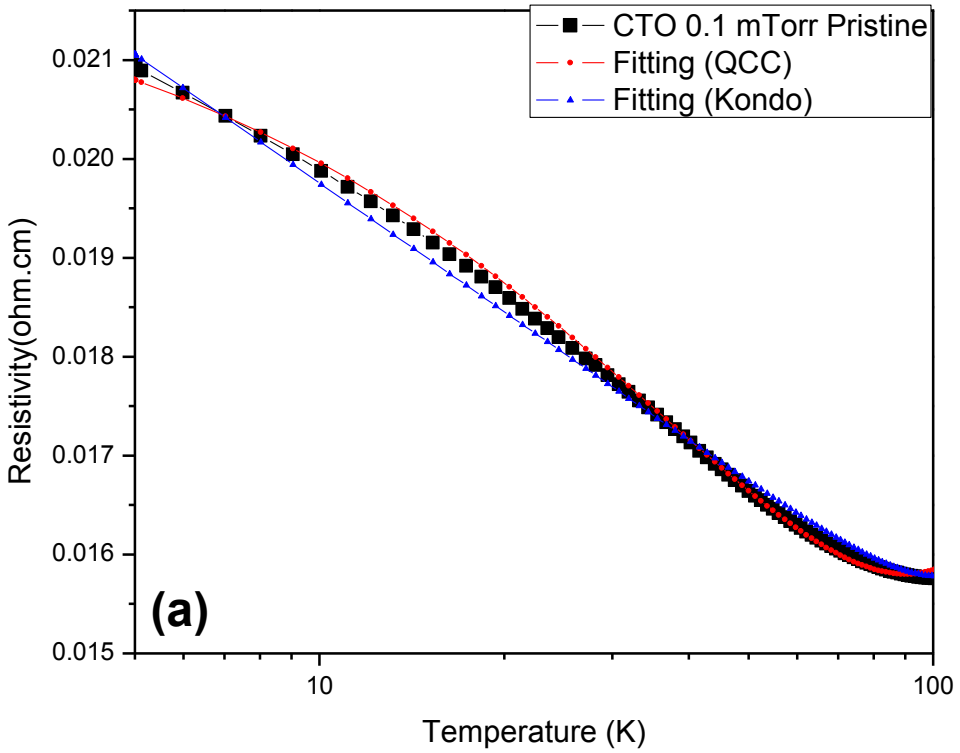
CTO 0.1 mTorr Pristine
Fitting (QCC)
Fitting (Kondo)
Resistivity(ohm.cm)
0.021
0.020
0.019
0.018
0.017
0.016
0.015
(a)
10
100
Temperature (K)

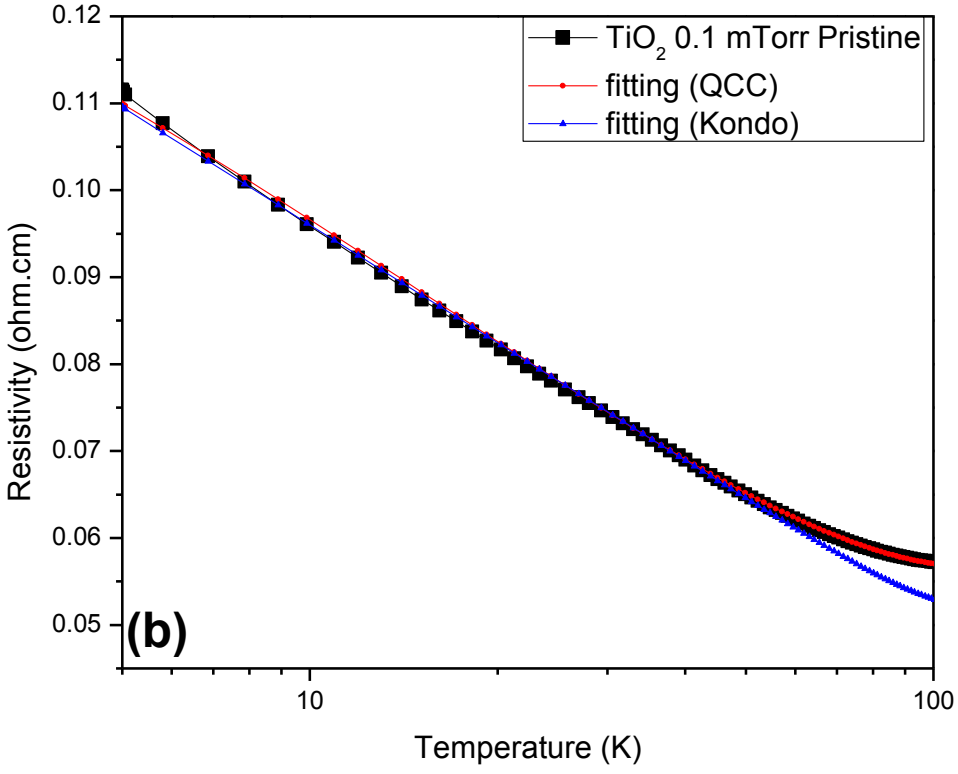
TiO2 0.1 mTorr Pristine
fitting (QCC)
fitting (Kondo)
Resistivity (ohm.cm)
0.12
0.11
0.10
0.09
0.08
0.07
0.06
0.05
(b)
10
100
Temperature (K)

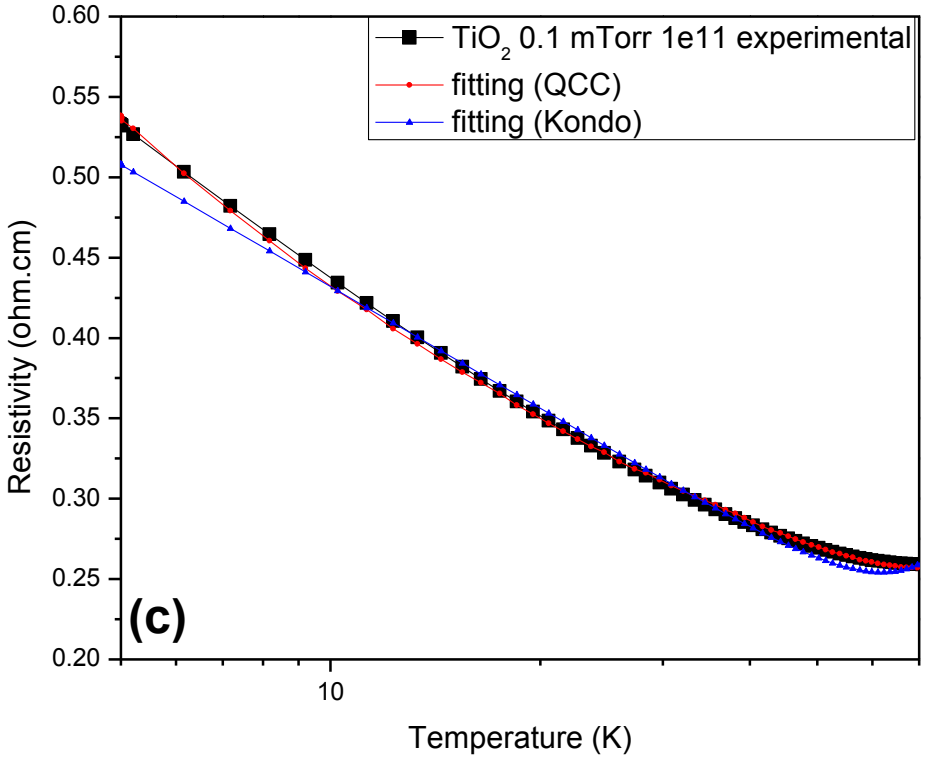

Fig.7.18 Resistivity as a function of temperature of $Ti_{1-x}Co_xO_{2-\delta}$ (x=0 and 0.05)thin film deposited under 0.1 mTorr oxygen partial pressure and irradiated with 100 MeV Ag^{7+} ions: (a) $Ti_{0.95}Co_{0.05}O_{2-\delta}$ (pristine), (b) $TiO_{2-\delta}$ (pristine) (c) $TiO_{2-\delta}$ irradiated with $1x10^{11}$ ions/cm^2 fitted with WL and REEI model for 3D system and Kondo equation.

Table 7.1 Fitting parameters of resistivity data considering Kondo equation.

	ρ_0 (Ω.cm)	ρ_1 (Ω.cm)	A	$(T_{min})_{expt}$	(T_{min}) Kondo	C
CTO 0.1 mTorr Pristine	0.535	9.55x10^{-2}	3.5x10^{-14}	103 K	102 K	0.045
TiO_2 0.1 mTorr Pristine	9.4	3	0.2x10^{-12}	115 K	115 K	0.015
TiO_2 0.1 mTorr 1x 10^{11} ions/cm^2	76	28	2.4x10^{-11}	72 K	62.3K	0.009

Table 7.2 Fitting parameters of resistivity data considering QCC.

	σ_0 $(\Omega.cm)^{-1}$	σ_1 $(\Omega.cm)^{-1}$	σ_2 $(\Omega.cm)^{-1}$	p	A	(T_{min}) QCC
CTO 0.1 mTorr Pristine	44.5	1.169	0.196	2	2.65x10^{-7}	89 K
TiO_2 0.1 mTorr Pristine	6.1	1.33	0.005	2	0.68x10^{-6}	113 K
TiO_2 0.1 mTorr 1x 10^{11} ions/cm^2	0.89	0.441	0.00055	2	0.87x10^{-5}	71 K

In pure normal metals, the mean free path (l) of the carriers is quite larger than the Fermi wavelength (λ_F). For this case, the transport properties of these metals can be explained by the semiclassical Boltzmann approach. In this picture, at $T < 0.1\theta_D$, where θ_D is the Debye temperature, the scattering of carriers by lattice imperfections leads to a low temperature resistivity following $\rho\,(T) = \rho_0 + AT^n$ behaviour, with ρ_0 is the residual resistivity, A is positive, and n is a positive integer (n = 3-5 for electron-phonon scattering, n = 2 when electron-electron scattering dominates). However, with increase in disorder in structure or composition, n can vary as well as the mean free path may become comparable to λ_F. In this scenario, a complete quantum-mechanical treatment, accounting for the wavelike nature of the carriers, must be applied. This

approach consists in adding some correcting terms to the low temperature conductivity known as quantum corrections to the conductivity (QCC) [Efros and Pollak (1985)].

QCC may arise from two distinct sources. First, there are effects coming from the self-interference of the wave packets as they are backscattered by the impurities or the other defects. This kind of self-interference may lead to additional scattering mechanism for an enhancement of resistivity. This picture is based on non-interacting carriers in a random potential approximation [Herranz et al. (2005)]. The other contribution arises from the renormalization of the effective electron-electron interactions and the subsequent modification of density of states at the Fermi level. Herranz et al. (2005) referred the former as weak-localization (WL) and the latter as the renormalized electron-electron interaction (REEI) to quantum corrections. Both contributions can explain the resistivity minima and the upturn in the resistivity at low temperature. Hence, we have considered the weak localization (WL) and renormalized electron-electron interaction (REEI) as the two main contributions to QCC. This holds good both for 2 and 3 dimensions. However, in our case the films are considered as 3 dimensional, as their thickness ~ 150 nm much larger than the mean free path (of the order of few nanometers). The temperature dependent resistivity considering the REEI and WL is given by:

$$\rho\,(T) = \frac{1}{\sigma_0+\sigma_1 T^{\frac{1}{2}}+\sigma_2 T^{\frac{p}{2}}} + AT^2 \quad \text{.....(2)}$$

where σ_0 represents the residual conductivity [Herranz et al. (2005)]. The other two terms present in the denominator, $\sigma_1 T^{\frac{1}{2}}$ and $\sigma_2 T^{\frac{p}{2}}$, account for the disorder present in the system and stand for the 3D REEI and WL corrections respectively: p is the temperature exponent for different scattering events. AT^2 represents classical Boltzmann term at low temperature in the expression of resistivity. The exponent, p = 2 or 3 represents the electron-electron coulombic interaction or electron-phonon scattering mechanisms at low temperatures, respectively [Herranz et al. (2005)]. We have fitted the ρ vs T data taking p = 2

which gives a good fitting (Fig. 7.18). Therefore, the low temperature resistivity behaviour below T_{min} is dominated by electron-electron columbic interaction. The fitting parameters are given in Table 7.2. Further it has been reported that in 3D regime, the REEI contribution to QCC dominates over WL whereas in 2D both contributions are of comparable magnitude. The fitting parameters in Table 7.2 show that σ_1 is dominated over σ_2 i.e. REEI is dominated over WL. The field dependence of the low temperature resistivity is significantly different and in principle it can unambiguously determine the nature of QCC. When by applying magnetic field, resistance decreases consequently gives a –ve MR, suggests WL term is suppressed. Instead the effect of field on REEI contribution leads to +ve MR. Therefore, after fitting to QCC, we have also examined the effect of magnetic field on resistivity at 5 K i.e. below T_{min}. The magneto-resistance (MR) [MR % = $(\rho_H - \rho_0)$ x 100 /ρ_0] at 5 K for both $TiO_{2-\delta}$ and $Ti_{0.95}Co_{0.05}O_{2-\delta}$ films (pristine and irradiated) deposited at 0.1 mTorr oxygen partial pressure are shown in Fig.7.19. $Ti_{0.95}Co_{0.05}O_{2-\delta}$ films show negative MR whereas $TiO_{2-\delta}$ films give positive values. The –ve magneto-resistance suggests that resistance after applying magnetic field decreases. This indicates the field destroys the wave coherence and reduced the self-interference that results the suppression of WL. However, the +ve MR can be obtained under magnetic field on REEI contribution only. This is because the spin splitting of electrons occur in a magnetic field and by orbital effects [Lee and Ramakrishnan (1985)]. QCC have been employed to explain the low-temperature transport properties of nonmagnetic disordered systems like doped semiconductors and metallic alloys. Negative magneto-resistance (MR) has been observed in these systems as suggested by the theory in the 3D limit which is consistent with suppression of WL factor by the applied field. However, in some magnetic systems, where the presence of a large internal magnetic field might suppress WL and then leave only REEI contribution. As a result, a +ve MR at low temperature would be expected. Manyala et al. (2000) have reported a +ve MR at low temperature for the $Fe_{1-y}Co_ySi$ and they

attributed it to the effect of the applied field on the REEI contribution. From the fitting, we clearly observed –ve MR in CTO where the WL is one order of magnitude lower than the REEI contribution well supports the literature. In TiO_2 and irradiated films, the WL term is much less than REEI.

For example we obtained σ_2 three orders and four orders of magnitude less than σ_1 .That means REEI is only term contributing to the resistivity behaviour. Observation of +ve MR in these films also supports the prediction of QCC. Thus, we confirm that the fitting parameters for ρ vs. T with QCC model well support the magneto-resistance as well. Although both films show RTFM, while in CTO both REEI and WL term contribute towards the resistivity at low temperature, in TiO_2, however, REEI is the only dominant parameter.

From the magnetism perspective, there are two key models that are used to explain the magnetic ordering in these materials, (a) Ruderman-Kittel-Kasuya-Yosida (RKKY) interaction (J_{RKKY}) and (b) Bound Magnetic Polaron model. In RKKY, the interaction between local moments is mediated by conduction electrons [Calderon and Sarma (2007, 2007 (a))]. According to bound magnetic polaron (BMP) model, the magnetic indirect exchange interaction takes place via shallow donor electrons which form a BMP with magnetic impurities, and overlap of these BMPs to create a spin-split impurity band [Coey et al. (2005)]. At sufficient donor concentration, when donor states merge with the bottom of the conduction band, the BMP model breaks down and RKKY interaction becomes operative [Calderon and Sarma (2007, 2007 (a))]. This RKKY interaction is supposed to compete with Kondo interaction according to Doniach phase diagram [Doniach (1977)] As we have observed a transition from insulating to conducting state showing minima in resistivity in case of TiO_2, CTO and film irradiated with $1x10^{11}$ ions/cm^2, we presume that both RKKY and BMP mechanisms compete with each other. However, for films irradiated with fluence $1x10^{13}$ ions/cm^2, the insulating behaviour with RTFM can be explained on the basis of BMP.

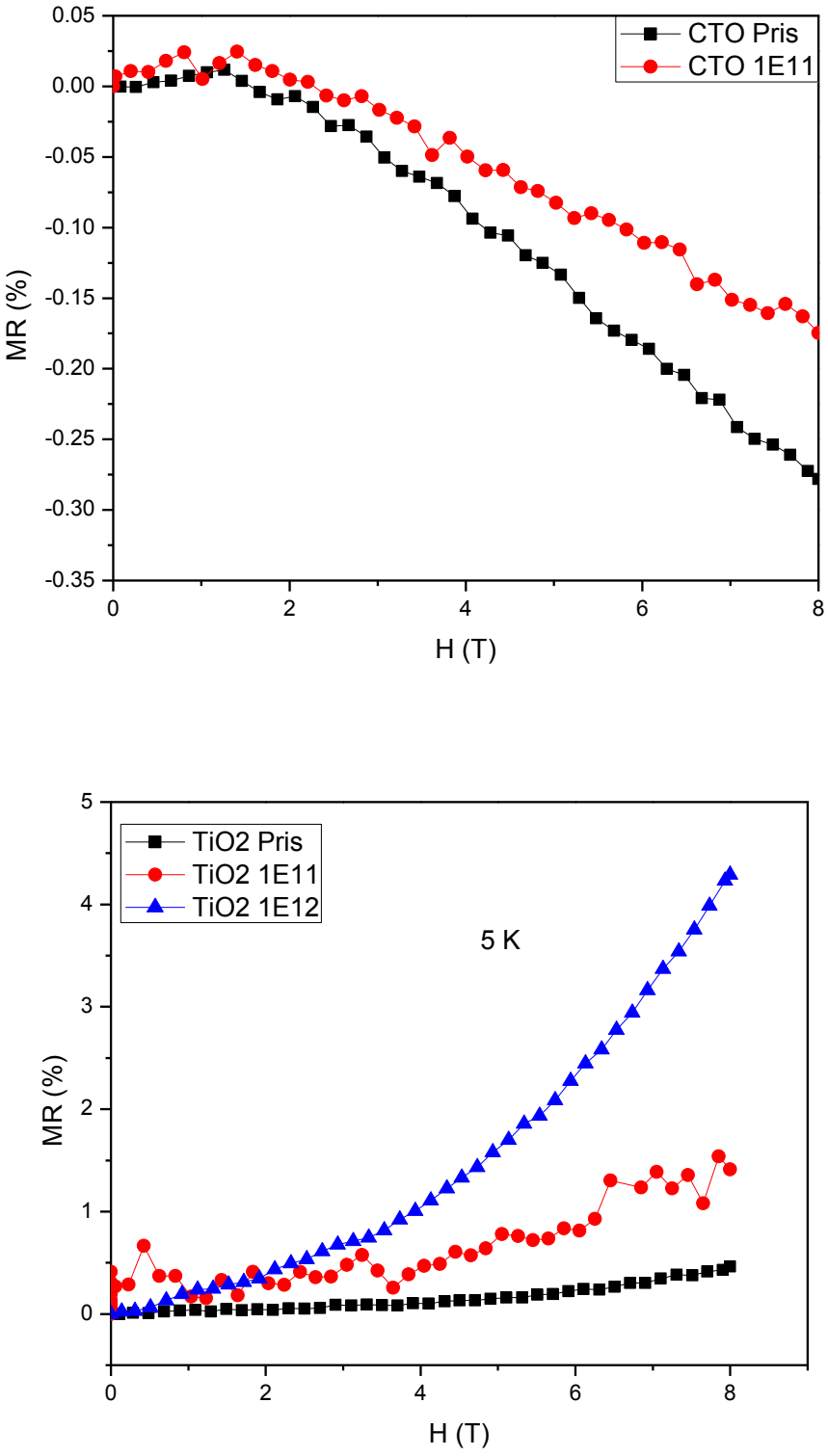

Fig.7.19 Magnetoresistance of $T_{1-x}Co_xO_{2-\delta}$ thin film ((a) x = 0.05 and (b) x = 0) at 5 K.

This type of existence of both BMP and RKKY models in dilute magnetic oxides have been proposed theoretically by Calderon and Sarma (2007, 2007 (a)). With ion irradiation the localization of electrons/defects is removed and makes the resistivity minima disappear. Consequently, the films become insulating whereas RKKY mechanism seizes and the BMP model may be operative to gives rise the ferromagnetic order.

7.4 Summary

The effect of swift heavy ion irradiation on structural and magnetic properties of ferromagnetic cobalt doped TiO_2 thin films deposited by PLD technique have been discussed. The film deposited at 0.1 mTorr oxygen partial pressure on Si substrate demonstrates rutile phase with higher degree of crystallinity. The crystallinity of the film persists even upto a fluence of 1 x 10^{12} ions/cm^2. Although, saturation magnetisation decreases with increasing fluence, ferromagnetic behaviour is still observed at room temperature even at a fluence of 1 x 10^{12} ions/cm^2. Fitting the exponential decay in x-ray peak intensity with ion fluence, the average track diameter is found to be ~ 4.2 nm. Magnetic measurements reveal an exponential decrease in the saturation magnetisation (M_s) with increasing ion fluence. Ion irradiation causes some magnetic disordered region surrounding the latent track that does not contribute to the observed magnetism. Using Poisson's equation, the diameter of the magnetic disordered region is estimated to be ~ 6.6 nm. We conclude that ion irradiation significantly induces magnetic disorder than structural disorder. In analogy to the track diameter calculation from the XRD data, for the first time we have shown the evidence of magnetic disordered region surrounding the ion path having random orientations of spins that increased with increase in fluence. High quality epitaxial TiO_2 and Co-doped TiO_2 films were grown on $LaAlO_3$ (001) single crystal using PLD technique. We have systematically varied the defect concentration in films during growth and thereafter with the use of SHI irradiation to study their effects on the structural, magnetic and

transport properties. The anatase structure is retained with changing oxygen partial pressure as well as ion fluence. Temperature dependence of resistivity of TiO_2 and $Ti_{0.95}Co_{0.05}O_{2-\delta}$ films deposited at 0.1 mTorr oxygen partial pressure reveal metallic behaviour, but with a resistivity upturn at lower temperatures. Magnetic measurements show TiO_2 and Co-doped TiO_2 films are ferromagnetic at 300 K. M ~ H shows an anomalous behaviour with ion irradiation of different fluence. M_s increases with fluence 1 x 10^{11} ions/cm^2 and then suddenly drops when irradiated with fluence 1 x 10^{12} ions/cm^2. Again the M_s increases for fluence 1x10^{13} ions/cm^2. Both TiO_2 and $Ti_{0.95}Co_{0.05}O_{2-\delta}$ films show increase in ρ with increase in oxygen partial pressure indicating decrease in oxygen vacancies. Resistivity data of the films deposited at 0.1 mTorr shows a minima at low temperature in pristine films that vanishes after irradiating with high fluence. We have fitted the resistivity data below minima using the proposed Kondo scattering model as well as QCC model and have found appreciable fitting in both the cases. However, the observation of ferromagnetism below T_{min} eliminates the Kondo effect. We have described the low temperature resistivity behaviour in $Ti_{1-x}Co_xO_{2-\delta}$ films by introducing quantum corrections to conductivity proposed for disordered electronic system for the first time. The ferromagnetism is governed by the competing RKKY and BMP mechanisms for the pristine and irradiated films at lowest fluence i.e. 1x10^{11} ios/cm^2. However, the magnetism in the films irradiated at 1 x 10^{13} ions/cm^2 may be explained on the basis of BMP model.